Spray flash evaporation SFE process: Identification of the driving parameters on evaporation to tune particle size and morphology

Emeline Lobry, Jean-Edouard Berthe, Denis Spitzer

Spray Flash Evaporation SFE process: identification of the driving parameters on evaporation to tune particle size and morphology

Emeline Lobry[a], Jean-Edouard Berthe[a], Denis Spitzer[a]

[a]**Nanomatériaux pour les Systèmes Sous Sollicitations Extrêmes** (NS3E) (UMR 3208 ISL/CNRS/Université de Strasbourg), **Institut franco-allemand de recherches de Saint-Louis** (ISL) 5, rue du Général Cassagnou BP 70034 68301 SAINT-LOUIS Cedex France

Corresponding author: elobry@unistra.fr

Keywords (max 6)

Spray flash evaporation – phase Doppler particle analyzer – crystallization – droplet measurement- polymorphism

Abstract

The spray flash evaporation process enables to recrystallize organic materials on submicron and nano scale and is basically based on the sudden depressurization of the solution from the superheated state to the primary vacuum through a nozzle. The immediate evaporation of the dissolved micro droplets results in the release of submicron or nanoparticles. As a first step, experimental data of recrystallization were collected for different energetic materials by varying the superheating conditions (injection temperature and pressure, solvent) and analyzing their effects on the materials properties (particle size, morphology and polymorphism). Then, the solvent spray is independently studied by measuring the velocity and the size of the generated

droplets. Key parameters to master particle size and morphology are identified. This study aims to identify the flash boiling and the spray characteristics. These results pave the way to some understanding of the process to be able to tune particles size and morphology.

Nomenclature

Nomenclature	Greek letters
Cp_l liquid heat capacity, $J.kg^{-1}K^{-1}$	λ: reference wavelength of 632.8nm
D_{32} mean Sauter diameter, µm	ρ_l liquid density, $kg.m^{-3}$
D nozzle diameter, m	ρ_g vapour density, $kg.m^{-3}$
h_{fg} vaporization latent heat, $J.kg^{-1}$	σ interfacial tension, $N.m^{-1}$
P_N pressure in the tank and in the nozzle, bar	σ_d standard deviation for particle size, µm
P_{sat} vapour saturation pressure, bar	µ mean diameter value; µm
P_V pressure in the vacuum chamber, bar	$\Delta\mu$ chemical potential
T_N nozzle temperature, °C	Abbreviation
T_{sat} saturation temperature, °C	ΔT_{SH} superheat degree, °C
U axial velocity of the spray, $m.s^{-1}$	CL-20 (2,4,6,8,10,12)hexanitro-hexaaza-tetracyclododecan
u_0 nozzle discharge velocity, $m.s^{-1}$	DSD Droplet Size Distribution
V radial velocity of the spray, $m.s^{-1}$	HMX: octogen, cyclomethylene tetranitramide
X_{vap} molar vaporization ratio	PDPA Phase Doppler Particle Analyzer
X position in the depth of the spray, mm	RDX 1,3,5-trinitrohexahydro-1,3,5-triazine
Y position in the radial direction of the spray, mm	RMS Root Mean Square

Z position in the axial direction of the spray, mm	SFE Spray Flash Evaporation Dimensionless numbers R_p pressure ratio ~~*Ja* Jacob number~~ ~~We_v vapour Weber number~~

1. Introduction

The crystallization process of submicron-sized particles is a longstanding challenge. Different routes can be considered either top-down to bottom-up. Most of these routes take place in liquid medium and need further steps such as filtration or drying to collect particles. The present process aims to combine all the operations in one. The Spray Flash Evaporation (SFE) was developed at the NS3E laboratory and it proves its ability to produce submicron or nanoparticles of energetic materials or drug compounds[1–5]. The basic principle is well described in literature[6–9].

The crystallization process taking place in the spray flash evaporation can be divided in different steps summed up in **Fig.1**. First the liquid dispersion is generated corresponding to an atomization step. It consists in producing a dense spray of droplets containing the precursors solutions. The quality of the spray depends on the nozzle geometry, the operating conditions (pressure, temperature and flowrate) and on the physical and chemical parameters of the solution (density, viscosity and surface tension). The aforementioned parameters will affect the flash conditions as well as the evaporation rate. Moreover, the solvent plays a main role in both dispersion conditions (viscosity, density) and flash conditions (thermal properties). The second step is the droplet-to-

particle conversion. This step is crucial for the removal of solvent. The flash evaporation induces a fast evaporation. The evaporation is promoted by the high-pressure difference inducing a fast gas expansion. The evaporation is governed by saturation pressure and thermodynamic properties of the fluid. This part requires to understand heat and mass transport phenomena but also crystallization of the precursor, governed by supersaturation, nucleation and growth of the particles. During the crystallization process, the solvent evaporates and then the solute concentration increases inside the droplet. The supersaturation is then reached quickly, and nucleation begins after an induction time. The main parameters responsible for the nucleation are the solvent, the solute concentration and the flash conditions (pressure and temperature). The success of the droplet to particle conversion is ruled by different characteristic times: the residence time t, the droplet drying time t_D and characteristic times related to the crystallization event t_C respectively the induction time t_{ind}, and the nucleation time t_N. The residence time must then be adequate to enable the global crystallization process. Finally, the resulting particles size can be affected by further agglomeration due to the reactor hydrodynamics. Drying is supposed to occur in the chamber.

One of the limitations of the spray flash evaporation is the choice of the solvent: the solvent must be able to solubilize the solute but also to be easily vaporizable in the operating conditions to promote fast nucleation and to provide a final dried product.

Hitherto, SFE process proved its versatility in the recrystallization of various submicron scale products of different types and morphologies (pure particle with different polymorphism, crystalline composites, semi-crystalline-composites or cocrystals [2]) and appears as a promising crystallization method, but mechanisms need to be investigated and the effects of the different

operating parameters on the materials properties and especially on the size and morphology are not straightforward because the independent role of each operating parameter is not obvious to assess. It is of primary importance to focus on the mechanisms involved and to suggest routes to tune particles morphology, size and properties.

Three parameters were investigated: the injection temperature, the injection pressure and the solvent type. Crystallizations of different secondary explosives were performed to obtain different particle sizes and morphology. Then a part focuses on the solvent spray study and flash boiling theory. Other experiments were carried out to study the solvent spray evaporation through the implementation of on-line metrologies. Fast camera and Phase Doppler Particle Analyzer (PDPA) were implemented to gain some insights on the droplet generation (size and velocities), the spray characteristics (width, angle, length), the flash phenomenon and subsequent evaporation.

Fig. 1: Various particle morphologies prepared by Spray Flash Evaporation.

Among the different on-line devices available, the PDPA was chosen for its ability to measure both velocities and droplet or particle sizes in dense medium. For pure solvent spray, the size, the axial and radial velocities of the droplets were measured under different operating conditions: injection pressure, injection temperature and solvent at different position inside the spray. These data sets aim to bring some knowledge on the effect of the operating conditions on the evaporation phenomenon and on the breakup mechanism of the droplets. Combining these data with thermodynamics modelling contribute to have an insight on the droplet size reduction and on the supersaturation depending on the product.

The combination of both studies provides first evidences regarding the tuning of particles size and morphology. The different parameters affecting particles are emphasized through the findings reached by these two sets of experiments. There are remaining questions about the SFE process to consider its scale-up: what are the effects of the different process parameters on the particles characteristics? The present paper objectives aim to pave the way of the identification of the key steps of the process and to underline the role of the main process parameters on the droplet size and velocities of the solvent spray in the light of crystallization results. This study is a first step towards the deep understanding of the involved mechanisms in this promising crystallization process.

2. Materials and method

2.1 Materials

The different solvents used were acetone from Höfer Chemie GmbH (99.5%), methyl acetate (>99%), ethyl acetate (>99%) and methanol (>99%) with HPLC grade provided by Carl Roth GmbH.

Some recrystallizations were also detailed. RDX, HMX and CL-20 were purchased from EURENCO. All compounds were dried in an oven at 70°C for 4h before further use.

2.2. Experimental set-up

Fig.2. **A)** Experimental set-up, **B)** schematic representation of the experimental set-up

The spray flash evaporation experimental set-up is presented on the **Fig. 2-A** and **2-B**. The spray flash evaporation process is composed of two different zones. The first is the high-pressure zone. The two tanks are pressurized between 20 and 40 bar with nitrogen depending on the operating conditions and contain either solvent or the solute in solution. The tanks are equipped with manometers and safety valves. They are connected to the nozzle which is a Brumstyl nozzle of 80µm with a ruby orifice. In the investigated conditions, the flowrates were respectively 10 $mL.min^{-1}$ and 7.5 $mL.min^{-1}$ for 40 and 20 bar respectively.

Just before the nozzle, the solution is heated between 110 to 160°C thanks to a heater band of 225 W. The temperature is controlled by a PID connected to the temperature sensor settled in the nozzle. The solution or solvent is released into the vacuum chamber. The vacuum was maintained by a pump of 63 $m^3.h^{-1}$. The two BK7 windows (15 mm of width, with a flatness of λ/10 to avoid disturbance of the laser light beam) enable the efflux visualization and monitoring inside the chamber.

To measure simultaneously the droplet size distribution as well as the velocities, a PDPA Phase Doppler particle analyzer was used (Dantec Dynamics, Denmark). The emission source is a FlowExplorer 2D with two diodes-pumped solid-state lasers of respective wavelength of 532 nm and 561 nm and a maximal power of 300 mW, the focal distance is set at 200 mm. The receiver optics for collecting the scattered light for dense spray are the PDA High-Dense with a focal distance of 310 mm with optic fiber and 3 detectors. The electronic device is the BSA P800 allowing the signal processing from optics to Doppler frequency. Each laser is adapted to a mono directional velocity measurement: the 532 nm for the *U* component corresponding to the axial velocity (Z direction) and the 561 nm for the *V* component, which is the radial velocity (Y direction)

as described in **Fig. 2-A** and **Fig. 3**. The laser intersection defines the ellipsoidal volume measurement of a diameter of 0.1mm and a length of 0.68 mm ie. 0.00356 mm^3. The receiving optics detect the scattered light produced by the droplet passing through the measurement volume. The signal is transmitted to the processor and converted to Doppler burst. The frequency shift of the signal is proportional to the velocity of the droplet in the given direction. The emission sources provide two incident beams of same intensity for each wavelength to improve the measurement of the frequency shift. The three photodetectors allow to measure the scattered light at different positions. The phase difference enables the estimation of the characteristic droplet size and size distribution. This measurement device is however limited to spherical particles. For each set of measurements, the device provides a sphericity coefficient. Measurement can be performed in the entire spray because the optical systems is set on a 3D- axis table with independent engines allowing the data acquisition at different positions. The initial position is defined at the tip of the nozzle. The consistency of the measurement was checked. After several trials, the number of droplets set is 20000. It represents the better option between acquisition time and accuracy.

Thanks to the 3D axes table with a 0.1 mm displacement precision, a quarter of the spray is scanned. **Fig. 3** depicts the measurement zone. The limitations are due to the current optical configuration. The window and the chamber designs do not allow to go lower and deeper without avoiding reflection on the wall of the chamber.

Fig. 3. Spray representation with the measurement zone depending on the XYZ axis set by the 3D axes table *(the origin is set at the nozzle outlet position and dimensions are in mm)*

The droplet size distribution (DSD) is obtained by analyzing the 20 000 validated samples measured. Different representative diameters can be drawn from the DSD. Some characteristic diameters can be calculated corresponding to different moments. Our choice for this specific application was based on two diameters: the *D10* (arithmetic mean-average) and the mean Sauter diameter D_{32} which is an average diameter defined as the same volume to surface ratio of a spherical droplet. It presents the advantages of taking into account the droplet surface, so the available exchange interface for mass and thermal transfer between phase and the volume droplet characterizing the available amount of matter. The Sauter mean diameter is defined by Eq. 1:

$$D_{32} = \frac{\sum_{i=1}^{n} n_i d_i^3}{\sum_{i=1}^{n} n_i d_i^2} = 6\frac{V_p}{A_p} \quad (1)$$

with n_i the number of droplets which size range from d_i to d_{i+1}, V_p the particle volume and A_p the particle surface for a spherical droplet.

So the D_{32} appears significant to characterize the solvent spray and the evaporation in the SFE process.

Among the different devices to characterize the spray, the PDPA is based on a flux sampling measurement: the individual drops pass through the cross section of the sampling region. This technique is sensitive to the particle flux.

Spray flow was also recorded by using a Phantom High Speed Multi Cam (Vision research AMetek, Germany) at 40 000 fps. The flow visualization allows to observe turbulence inside the spray. The frames are binarized and the spray angle is extracted by using a homemade code using MATLAB.

The spray was lighted with a spot. The position and intensity of the lighting is the same for all the set of experiments. As a consequence, the contrast differences enable to compare qualitatively the effect of the operating conditions (P_N, T_N and solvent).

2.3. Fluids characteristics

Fig.4. Saturation curves for different common solvents

Fig. 4. depicts the saturation curves for different solvents. During the introduction in the vacuum chamber, the solvent experiences a rapid expansion process. When the solvent pressure becomes below the saturation pressure, flash boiling occurs as the formation of bubbles within the liquid core. When solvent is below 100°C, methanol exhibits a lower pressure compared to acetone or methyl acetate. The methanol spray is anticipated to experience flash boiling at lower pressure compared to acetone. The relationships between the solvent saturation pressure to ambient pressure and the solvent temperature to boiling point temperature are key parameters to explain the difference of spray observation [10]. In pink, the classical operating conditions performed in SFE are depicted and **Table 1** provides the physical properties of these solvents at ambient conditions.

Table 1. Physical properties of different solvents.

2.4. Solvent spray operating conditions

Table 2 sums up the different operating conditions investigated for the solvent spray study. The results are presented in section 3.3. To compare the different solvents, data are collected in the 0-0-Z direction for methanol, methyl acetate and ethyl acetate.

Table 2. Operating conditions for the solvent spray tests.

2.5. Crystallization experiments

The different operating conditions for crystallization are reported in Table 3.

Table 3. Operating conditions for the recrystallization of different explosives (P_V=5 mbar, nozzle 80 µm).

2.6. Particles characterization

Morphologies of the composites are imaged by a FEI Nova (USA) NanoSEM 450 Scanning electronic microscopy (SEM) equipped with a field emission gun operating at 10 KW. Samples were covered by a thin gold layer (8 nm). The chamber pressure amounts $<10^{-5}$ mbar during the measurements. Sizes measurements were made manually over at least five hundred particles per sample within the software Gwyddion then a lognormal fit is applied on the particles size distribution (PSD):~~geometrical mean and multiplicative standard deviation (dimensionless~~) the mean value μ and the standard deviation are reported [16]~~ are reported here and written as ''mean(SD) unit". a~~s well as the polydispersity characterizing the width of the distribution.

X-Ray powder diffraction (XRPD) was conducted by Bruker (Germany) D8 apparatus with LinxEye detector (copper anode λ=1.541056 Å) in Bragg-Brentano geometry.

3. Results

3.1. Recrystallization of organic compounds

Fig. 1 introduced the main parameters affecting crystallization in SFE. The driving force of the crystallization process is the supersaturation. This parameter depends on the solubility and the rate of evaporation in the spray flash evaporation process. In this part, a parametric study with different organic materials is presented. The three compounds are secondary explosives used for civilian and military applications. The operating conditions and solubility are reported in **Table 3**.

All the details of the crystallization results are available in the supplementary materials part. **Table 4** presents the results of particle characterization for the different crystallizations.

Table 4: Particle size and morphology of the different explosives obtained by SFE

3.1.1. Effect of T_N

Particle size decreases by increasing temperature. This result was previously noticed by Risse [1] for 1 wt% RDX solution in acetone sprayed at 40 bar. This is clearly noticeable for spherical particles such as RDX and CL-20. For HMX, at 20 bar the phenomenon is obvious. At 40 bar, needle shape particles of HMX are produced and highest temperature gives thinner rods.

3.1.2. Effect of P_N

The decrease of the injection pressure enables to obtain smallest particles size with RDX and CL-20 materials, solvent and injection temperature being constant. In the case of HMX in

acetone, different morphologies of particles were noticed depending on P_N. HMX-1 and HMX-3 obtained at 40 bar and two different temperatures (160°C and 110°C) provide rod shape particles where as HMX-2 and HMX-4, obtained at 20 bar, are respectively plate-like and spherical submicron particles (SEM pictures on **Fig.S2 A** and **B)**. The pressure affects here directly both size and morphology. However, the polymorphic forms obtained are either γ or mixture of γ and α which aged all in α after 5 months according to the XRPD patterns.

The injection pressure P_N does not change the superheating conditions but also the flowrate of the spray in the SFE process. At the same time, the other parameters such as the temperature or the vacuum pump flowrate, are kept constant leading to build-up of solvent inside the crystallization reactor. As a consequence, the increase of particle size occurs probably due to the capacity of the pump to get rid of solvent vapors gathered in the crystallization reactor. It might be responsible for a longer contact time between solvent and solute, increasing the crystallization time and then particles growth.

3.1.3. Effect of the solvent

The solvent influences the solubility of the precursors and the evaporation conditions both controlling supersaturation and its kinetic. In the case of RDX, adding water to acetone conducts to same mean particle size but narrower distribution despite the decrease of the solubility of RDX in the solvent.

In the case of HMX, the addition of water changed not only the size of the particles but also the morphology (HMX-1 and HMX-5). Spherical particles of submicron size were obtained by changing

the solvent as shown **Fig.S3-A**. The comparison is not trivial. Solvent simultaneously changes both evaporation conditions and supersaturation. Water is an antisolvent, decreasing HMX solubility [13]. The solvent choice can also influence the particle polymorph like HMX-4 and HMX-6. In the first case, acetone is used with a solubility of 2.8wt.% for HMX whereas it drops to 0.49wt.% in the case of methyl acetate. The degree of supersaturation takes again a higher value. HMX-4 presents the α- form whereas the HMX-6 is a mixture of γ and β as presented in **Fig.S3-C**. However, the particle size distribution of both samples are almost superimposed despite the lowest solubility in HMX-6 (**Fig.S3-B**).

The effect of solvent is tested and presented on **Fig.S5** in case of CL-20. It is twice more soluble in acetone than in methyl acetate but the solubility is quite high in both solvents. Same polymorphs were obtained and a slight decrease in mean particle size and a shift to the smallest size is obtained for the CL-20-6 compared to CL-20-4. The solubility of CL-20 in methanol is very low compared to solubility in acetone or methyl acetate (**Table 3**). The particles obtained in the same operating conditions than for acetone (CL-20-1) present a larger mean particle size and size distribution. Different polymorphs are formed depending on solvent used in same operating conditions (T_N,P_N).

3.1.4. Findings in crystallization of pure organic compounds

There is a lack to understand particle size and polymorph change. It seems important to study the evaporation conditions to understand the results. Intuitively, evaporation rate is promoted by increasing temperature T_N. As a result, for a droplet of precursor in solution, the solvent

evaporates faster and the supersaturation is reached in a shorter time if the temperature raises. The particles do not have enough time to grow and are therefore smaller. The pressure P_N does not seem to be directly related to the evaporation but is responsible for the flowrate and gas solvent buildup inside the chamber.

The solvent choice appears as a key parameter in the crystallization. It will concomitantly affect the solubility of the compound and the thermal properties responsible for evaporation conditions. Both parameters control the supersaturation inside the droplet which is the driving force of the crystallization process.

So before proceeding to a deep explanation of our results, the second part of this results section is devoted to the evaporation study of the solvent spray.

3.2. Short state of the art on spray flash evaporation

3.2.1. Literature

Flash atomization was studied for fuel oxidant mixing for combustion, desalination process [17–20] and for direct-injection gasoline engine with different fuels such as alcohol fuel [10]. Spray flash evaporation refers as violent evaporation phenomenon occurring in a liquid undergoing a sudden pressure drop until at least bubble pressure. The liquid is initially subcooled, and the liquid bulk is brought to a superheated state. Mass transfer is proved to be ten to twelve time higher than for classical evaporation [21]. It is first mentioned in literature since the 1960s by Brown [22] who described spray flash in different types of nozzles for water and freon by tuning injection

temperature or pressure and providing first spray observations. The key finding conclusions were the decrease of the droplet size by increasing injection temperature and the larger droplets size with distance from the spray axis.

The injection temperature plays a huge role on the spray : the temperature raise leads to an increase of the spray angle in the downstream direction[23–25]; the axial velocity profile tends to become uniform [26] and the maximum velocity at a given axial position is located at the jet centerline in the conditions used (Table 5). In the spray, the droplet velocities decrease in the radial direction but the rise of the RMS of the velocities indicate increase of fluctuations.

The second main parameter is the injection pressure P_N. Up to a certain value, the rise of the injection pressure results in a decrease of the obtained droplet size [27].

Some authors reported the effect of a third parameter, the discharge or backpressure P_V, on the stability of the jet which decreases by reducing the chamber pressure. Most of the reported studies occur at a discharge pressure corresponding to the ambient pressure and very few studies were carried out under vacuum [27,28]. **Table 5** sums up the operating conditions for flash evaporation studied in literature.

Table 5. Different studies of spray flash evaporation in literature and their operating conditions.

It reveals that there is a lack of information in the literature regarding the operating conditions used in the spray flash evaporation SFE process. Spray flash boiling is characterized by an increase of the spray angle and a decrease in the mean droplet size and driving pressure. Consequently, the flash spray phenomenon occurs at high temperatures or large pressure drops [30]. The spray is characterized by its penetration length and its angle.

3.2.2. Theory of flash evaporation - mechanism

Flash atomization is based either on temperature or pressure difference. Two parameters described the superheat level in literature:

- the temperature difference between the solvent injection, T_N and the saturation temperature at the assigned backpressure $T^{sat}(P_V)$ named superheat degree defined by Eq.2:

$$\Delta T_{SH} = T_N - T^{sat}(P_V) \quad (2)$$

- the pressure ratio R_P between the saturation pressure at the injection temperature $P^{sat}(T_N)$ and the backpressure P_V defined by Eq.3:

$$R_p = \frac{P^{sat}(T_N)}{P_V} \quad (3)$$

R_p is directly related to the difference in chemical potential $\Delta\mu$ which represents the generalized driving force for the phase transition process and bubble nucleation.

Flashing phenomenon may occur either inside or outside the tank, the connecting pipe or the nozzle itself, i.e. external or internal flash. The saturation induces the generation of large number of bubbles inside the liquid phase. When the jet is released, a combination of hydrodynamic instabilities and thermal non-equilibrium conditions in the flow expands the jet. Violent and explosive characteristics of the jet cause its break-up into smaller droplets. Bubble growing mechanisms can be divided in two regimes. In the first regime, the pressure inside the bubble is great enough that it can push the liquid aside and increase the size of the bubbles. It refers as "inertia-controlled growth" regime. In the second regime, the heat from surrounding liquid is transferred to the liquid adjacent to the interfacial region of the liquid and vapor and then the

phase changes from liquid to vapor. This growth mechanism referred as “heat transfer-controlled growth”. Bubble generation and growth turn the liquid flow into a bubbly two-phase flow.

Different flashing regimes [31] can be described depending on the location of the atomization inside or outside of the nozzle.

In external flashing, the jet flows from the nozzle as a single-phase jet and atomization occurs at some distance from the nozzle exit. The length of the intact liquid core corresponds to the delay time during which bubbles are formed and grow causing the jet to disintegrate. This external flashing phenomenon is unstable and difficult to control. The geometry of the spray is ruled by balance forces acting on droplet: at the immediate nozzle exit, the spray angle is determined by capillary or aerodynamic instabilities depending upon the efflux velocity. Then, surface tension, aerodynamic forces and thermodynamic instabilities interact and are responsible for the spreading of the spray. At location in the spray, heat transfer and flow fluctuation depending on the hydrodynamics may enhance or inhibit flash boiling.

In internal flashing jet, the two-phase flow already settles within the nozzle due to high superheat degree. Three regimes can be distinguished: bubbly, slug and annular flow. Jet disintegration takes place directly at the nozzle outlet. This indicates upstream bubble nucleation: either by homogeneous nucleation via kinetic processes within the bulk liquid or by heterogeneous nucleation due to the wall materials roughness of the nozzle or to the nozzle geometry. The spray angles become wider by increasing the degree of superheat. The initial lateral spreading of the spray is basically controlled by nucleation.

A microexplosion in drops model was first proposed by Razzaghi [32]. It assumes that the process is described as a subsequent progression of bubble nucleation inside droplets which then grow.

Droplet breakup through bubble disruption and droplet evaporation. Then, secondary droplets follow the same steps forming the spray. When flashing occurs, it becomes the dominant breakup phenomenon. The onset of the phase change process occurs at nucleation sites. It is at these locations that the metastable liquid can form vapor bubbles which grow until the system is once again stable. Nucleation sites may be either in the form of dissolved gases or impurities. The process enters in the bubble growth phase. The boiling conditions continue until the latent heat absorbed by converting the liquid to a vapor is balanced by the excess energy of the liquid which initially rendered it thermodynamically unstable. The liquid is broken into small droplets and the effect of surface tension becomes significant.

For highly superheat conditions, corresponding to $Rp > 50$, a shock wave structure surrounding the dense jet core has been observed [29]. It could be related to nucleation inhibition due to vigorous evaporation occurring directly from the surface of the metastable liquid jet. Indeed, authors demonstrate that above this threshold value, operating conditions do not have effect on the drop size and spray angle [29].

3.2.3. From spray flash evaporation to the SFE crystallization process

Spray flash evaporation was studied in literature and different correlations based on the estimation of droplet size, velocity distribution or spray characteristics (jet spreading angle or penetration length) are available in the literature. These correlations assumed a complete external flashing (metastable liquid core disintegrated completely at a certain distance of the nozzles) so flash boiling is solely controlled by bubble growth rate (see section 3.3.1). These

correlations are based on experimental data and details are provided in different publications[33] [34]

Generalization was attempted by Lamanna *et al.* [29] which point out that the driving force is the R_p ratio rather than ΔT_{SH}. A correlation was proposed based on the validation of two hypotheses: there is a direct link between bubble nucleation rate and flash boiling. Suggesting the maximum expansion of the spray is limited by the nucleation kinetic in confined volume and the residual superheat is relieved by evaporation. Secondly, the threshold of fully flashing is directly linked to the barrier of energy nucleation. So, the ratio between both energies must be below 1. They established a correlation based on measurable parameters for different kind of fluids and linked the spreading angle ϑ and the mass flux m to the $log\left(\frac{R_p^2\theta^3}{m^2}\right)$. Wettability and surface roughness effects are yet not taken into account whereas Günther and Wirth [35] demonstrate that polished surface required much higher superheat degree to sustain active nucleating cavities and hydrophobic zones acting as promoters of nucleation sites.

A noticeable work was performed about spray flash evaporation in literature. However, compared to the studies performed in literature dealing with spray flash evaporation, the classical operating conditions used in the SFE crystallization process are beyond the scope of the injection temperature or pressure and backpressure used. Indeed, the superheat degree ΔT_{SH} is very high (above 80°C) and the pressure ratio R_p also because moderate injection pressure (20-40 bar) to vacuum backpressure are reported. Moreover, solvents are also different. The only case studied reported dealing with crystallization is the work of Gebauer *et al.* [36,37] where the first part of their process requires a flash evaporation. The system was KCl/water but the main purpose ~~of~~

~~this study~~ was to obtain large crystals: the droplets flowed in a sump where the crystals growth occurred until mm whereas our goal is to produce submicron and even nanometric particles.

In crystallization, supersaturation is the driving force. In the case of SFE, it depends on the solubility of the compound and on the evaporation conditions as highlighted in **Fig.5**. The solute concentration inside each individual droplet increases depending on the evaporation rate and the supersaturation is reached. As consequence, first nuclei appear according to a stochastic process ie presence or numbers of nuclei are randomly distributed between droplets. Nucleation kinetics is directly related to the supersaturation. The principle is to create a huge number of nucleation sites by creating a huge number of finely divided droplet undergoing a fast evaporation. Particles are progressively obtained from the evaporating droplets and growth is limited. The study of the crystallization kinetics are beyond the scope of the current work and will be studied in the future. Before going into details of the crystallization, the goal is to identify the main parameters influencing the evaporation and to master it to gain some knowledge on the SFE process mechanism. This first understanding stage is crucial and mandatory to go deeper in the supersaturation and then nucleation control. The solvent spray study then enables to identify parameters which tune evaporation through droplets size, velocities and geometrical spray characteristics measurements. The purposes of this work are (1) to evidence the flash mechanism in the SFE specific conditions, not studied in literature; (2) to highlight the process parameters which affect the spray morphology: spray length, angle of the spray and droplet size and droplet size distribution; and (3) to identify the main parameters tuning the evaporation conditions and how they affect the particle size and morphology.

Fig. 5: Schematic representation of the SFE crystallization process – first understanding stage: from droplet evaporation to the final particle

3.3. Study of pure solvent spray

3.3.1. Thermodynamics

As a first step, flash calculations were made to calculate the equilibrium temperature and the evaporation rate when the liquid flows into the vacuum chamber. As inlet conditions, the vacuum pressure P_V is set at 5 mbar and the solvent operating conditions, T_N and P_N were set according to **Table 2**. This calculation allows us to determine the superheat degree ΔT_{SH} defined by Eq.2 and the molar vaporization ratio X_{vap} defined by the ratio between the vaporized moles to the initial moles.

The results are reported in the **Table 6.**

Table 6. Calculation of the relevant parameters in the operating conditions of the study.

This basic calculation provides a first insight in the solvent evaporation which must be complete to obtain dried particles. It corresponds to the thermodynamic equilibrium reach at the nozzle outlet. It does not take into account the dynamic evaporation process occurring inside the crystallization reactor. The heat capacity must be quite high whereas the enthalpy of vaporization must be low to ensure an efficient heat transfer.

Table 6 assumes that the evaporation rate is higher applied in the order acetone > ethyl acetate > methyl acetate > methanol for the same operating conditions in the SFE process. In addition, the vaporization ratio increases by increasing the superheat degree ΔT_{SH}.

Part 3.2.3 emphasizes the importance of mastering the spray evaporation. Intuitively to obtain nanoparticles, the goal is to create a huge number of nucleation sites and to avoid or limit the growth of the particles. This is achieved by creating a huge number of droplets finely divided undergoing a fast evaporation and succeeding in the appearance of numerous nuclei, producing nanoparticles. In our system, depending on the conditions of non-flash boiling or of flash boiling, spray could be generated according to the R_p value (**Fig. 6**). For non-flash boiling sprays, the break-up phenomena are governed by inertia force, surface tension, viscous forces and drag forces. For flash boiling sprays, the break-up mechanism must comprehend the bubble formation and expansion within the bulk liquid. The solvent undergoes a depressurization from a high-pressure condition to vacuum pressure in our case. When the pressure is below the solvent saturation pressure, gaseous bubbles are generated inside the droplets. These bubbles expand and disintegrate the liquid into smaller ones. **Fig. 6** represents the relationship between the dimensionless number R_p (Eq.3) and the superheated degree ΔT_{SH} (Eq.2) identified in the section 3.2.2 as key parameters for the flash evaporation. Both parameters are characteristic of the structural behavior of the observed spray. These two characteristic numbers are linked by a logarithmic relationship and are similar in principal. The full-pink points depict the operating conditions used in crystallization taking place in the Spray Flash Evaporation process and already published by our laboratory. In their publication Zeng *et al.* [10] observed flash-boiling spray at P_V/P_{sat} below 1 corresponding to the reverse of R_p defined as Eq.2.So, flash boiling conditions were reached in the conditions used.

Fig. 6. Relationship between R_p and ΔT_{SH} for different solvents.

In literature, a comparison of the spray at consistent R_P leads on similar spray structure [13]. However the transition to the fully flashing regime varies depending on the fluid and applied backpressure [29]. Highly superheated conditions are defined for R_P value beyond 50 where the total vaporized mass increases. The conditions tested for recrystallization by SFE significantly exceed this value as shown in **Table 6** and it is very likely that the rapid expansion of the flow right at the exit of the nozzle is not yet matched with the relaxation of the system until reaching thermodynamic equilibrium and sustained vapors take place within the two phases flow region. The maximum flowrate is limited by the sonic conditions given by Chapman-Jouguet. This supersonic expansion is terminated by a shock wave to match the vacuum pressure set in the chamber. This phenomenon of shock wave is described and commented in different publications [28,29,38]. Increasing the R_p corresponds to an increase of bubble nucleation. The total vaporized fuel mass increases as well as the associated vapor pressure. The resulting supersonic expansion results in a wider shock structure of increased strength. According to this literature study, it is highly possible that the spray undergoes shock wave in the SFE process.

3.3.2. Visualization of the spray

Fig 7 depicts the visualization of the acetone spray at same time scale for different operating conditions. Pictures are provided at different time (T0 to T3) to appreciate the movement of the fluid. The spray efflux is disrupted and lots of recirculation above the nozzle are

observed. These fluctuations depends on the operating conditions (temperature, pressure) and on the design of the used chamber (see **Fig. 2A**). Qualitative interpretations can be deduced from these frames and records.

Fig. 7. Acetone spray under different operating conditions at T0, T1 (3350ms), T2 (18975ms) et T3 (74975ms)

First, temperature raising, *ie* the supersaturation degree at fixed pressure, promotes turbulences and flow disturbance as observed at 160°C and 110°C on the pictures taken at different time scale. The hydrodynamic of the spray is influenced by the superheating degree: increase the superheating degree leads to lots of disturbance in the nozzle area as shown on the pictures and more generally inside the complete chamber.

Then, the effect of the pressure can also be investigated. As stated before, the nozzle pressure P_N is directly related to the spray flowrate. A less dense spray is generated by decreasing the pressure as supported by the pictures on Fig.7 at 110°C for both pressure value displaying less brightness. The amount of evaporated solvent is then lower and limits solvent buildup avoiding too much disturbance in the crystallization reactor.

The frames were retreated to extract the spray angle ϑ at the different conditions for acetone in **Table 7**. An example of treatment is provided in **Fig. S6**. The given value corresponds to a mean value obtained on the attested frames.

Table 7. Spray geometry for acetone in different operating conditions.

The spray angle is slightly influenced by the pressure and not affected by the superheating degree in these operating conditions. As stated by Lamanna *et al*., above a threshold value of R_P, the operating conditions does not impact the spray angle [29].

Recordings were also collected for different solvents and different operating conditions. **Fig.8** displays spray pictures of different solvents in the same operating conditions (P_N, T_N). Methanol is the least volatile and exhibits a more concentrated spray with lots of eddies around and above the nozzle. This causes the extraction of spray angle impossible with high background noise. Ethyl acetate presents a higher vaporization ratio than acetone according to **Table 6**. Fig. 8 shows that the spray geometry is tuned by the solvent thermodynamic properties. Indeed, the spray penetration is shortened with the evaporation and is correlated to the molar vaporization ratio X_{vap} provided in Table 6. A large amount of the spray can be as a first estimation considered vaporized at respectively 1.7, 3.1 to 3.8 cm below the nozzle at 20 bar and 110°C for respectively the ethyl acetate, acetone and methanol. It suggests that solvent evaporate inside the crystallization reactor.

Fig. 8. Visualization of the spray for different solvents and operating conditions

3.3.3. Effect of the injection temperature T_N on the spray flash evaporation of acetone

3.3.3.1. On the mean droplet size

The operating parameters studied are described in **Table 2**. **Fig.9A** presents the effect of the temperature on the *D10* along the Z-axis at the center of the spray (X=0, Y=0). DSD respectively at Z=0 and Z=-11 are also described in **Fig.9B**. A full 3D representation of the spray (quarter) is

available in the supplementary material part (**Fig. S7**).Evaporation of the droplets is evidenced by the mean diameter decreasing along the Z-axis. Smaller mean droplet size distribution at the tip of the nozzle are measured with the increase of T_N. However, the droplet distribution of the spray at 110°C displays a higher polydispersity along the Z axis**.** At high superheat degree, the DSD decreases. Uniform and smaller droplets are obtained faster. The evaporation is enhanced.

Fig.9. A) Evolution of the *D10* depending on T_N along the Z-axis at the center of the spray (X = 0, Y = 0) B) DSD depending on the temperature at 0-0-0 and 0-0-(-11).

Fig. 10 depicts the size variation of the droplets for different X position along the Y axis at Z =-11. The analysis zone is drawn in red in the figure. The droplet size is rather homogeneous at T_N value of 160°C and 140°C with *D10* value ranging respectively from 1 to 0.7µm and 1.6 to 1µm. At 110°C, a drop is noticed from 3 to 1µm.

Fig.10. Evolution of the D10 at Z =-11mm in the radial direction for different X.

3D representations of the droplet size of the spray are available in the supplementary materials and different 2D plans (**Fig. S8 to S10**). There is a maximum in droplet size between -2 to -8 mm after the nozzle. Maximum droplet sizes were obtained in a zone close to the centerline of the spray whatever the applied temperature. Sauter mean diameter is larger at the center of the spray and decreases from the center to the edge of the X axis. This information provides some insight on the evaporation and on the droplet generation mechanism. Interestingly whatever the temperature, it seems that there are larger droplets at Z = -12.5 mm. These results are confirmed

by the spray visualization in the three plans: red zone corresponding to the larger droplets can be noticed in the ZY and ZX plans.

By increasing spray temperature, higher ΔT_{SH} are reached promoting the expansion phenomenon. However, smallest droplets sizes were measured near the tip of the nozzle suggesting a faster evaporation at higher temperature.

3.3.3.2. Effect of the injection temperature T_N on the spray flash evaporation of acetone on the axial velocity U

Fig11 and **Fig. S7-A** depict the effect of the temperature T_N on *U,* the axial velocity. First, whatever the temperature, the axial velocity is maximal at the center of the spray, in the nozzle axis. The temperature T_N acts on the spreading high velocity zone as depicted on the 3D representation (**Fig. S7A**. and in XY plan in **Fig.S9**). The zone of high kinetic energy is larger by increasing the superheating degree and more intense regarding the *U* value provided **Fig.11**. This observation is in accordance with the literature.

Fig. 11. Mean axial velocity *U* along the Z axis in the 0-0-Z position.

To illustrate, as in the previous part, *U* profile at Z=-11, at different X position along Y axis are depicted in **Fig. 12** It represents a vertical plan. Maximum velocities are obtained in the centerline of the jet.

Moreover, increasing the temperature increases slightly the mean value of the axial velocity as suggested in **Fig.11** for Z values below -15 mm. These observations are in accordance with the

location of the highest Sauter mean diameter observed. Combining these results with the mean diameter value emphasizes that faster evaporation occurs by increasing the superheating degree.

Fig.12. Mean axial velocity U at Z =-11 for the different T_N for the acetone spray at 40 bar depending on the radial position Y and for different X.

Table 6 shows that an increase in the T_N affects the superheating degree ΔT_{SH} and the vaporization ratio X_{vap}. The observations of larger spray by increasing the temperature assume that droplets probably undergo an expansion phenomenon leading to a breakup of droplets into smaller ones. This mechanism is promoted by evaporation: the high superheating degree and pressure drop generate bubbles inside the droplets which grow and burst. This mechanism promotes the spray expansion with temperature due to the highest X_{vap}. The increase of the axial velocity is probably related to the more violent evaporation.

3.3.3.3. Effect of the injection temperature T_N on the spray flash evaporation of acetone on the radial velocity V

Fig. 13. Mean radial velocity *V* along the Z axis in the 0-0-Z position.

Fig.13 represents the radial velocity in the jet centerline for the three temperatures of the spray. At the highest temperature, close to the injection, *V* reaches high values but remains close to zero in a large part of the spray. The 3D representations in **Fig S8-C** display the variation of the radial velocity and the **Fig.S11** provides evolution in the different plans of the spray. The radial velocity

is maximal around the tip of the nozzle and at the edge of the spray where there is a zone of high kinetic energy. It defines a cone. At T_N=110°C, the radial velocity, measured only at the tip of the nozzle in the XY plan, increases in the Y direction as well as the X direction. At T_N=140°C, the red zone is larger. The same localization is observed but it defines a larger zone in Z axis and it is also larger in Y and X directions. It is characteristic of the width of the high kinetic zone in the spray and sustains the droplet burst. At higher temperature, the same zones are always measured but the limiting measurement abilities of the device is often reached (limiting maximal velocity reached) which makes the data collection difficult at some specific locations. Increase the temperature seems to raise the radial velocity at the edge. This is in relation with a higher superheating temperature.

Fig.14 represents the different radial velocity *V* measured for the three temperatures in the Y direction, regarding the location of the emission and reception sources as described in **Fig. 3**. The radial velocity is close to zero at the center of the spray where the axial velocity *U* is maximum.

Fig.14. Effect of TN on the radial velocity V for different positions at Z=-11mm (left) and Z = -4mm (right)

The smallest size of the cone is evidenced at 110°C because high radial velocities are measured from the axis tip directly suggesting a limiting spray expansion.

3.3.3.4. Temperature effects on the acetone spray - conclusion

The acetone spray was studied in terms of droplet size and droplet velocities for a constant inlet pressure P_N and under different nozzle temperatures T_N. The spray cone is clearly impacted by the superheat degree. The increase of temperature leads to smaller droplet size in the spray suggesting a faster evaporation. The maximal axial velocities reached are in the same order. However, there is a wider zone of high velocities for higher superheat degree. ΔT_{SH} enhances the evaporation phenomenon as shown by the high droplet velocity probably due to the subsequent droplet burst. The turbulence surrounding the spray droplets are probably linked to the shock as well as the flash boiling leading to bubble nucleation and drop bursting. This improvement of the vaporization phenomena will be studied regarding the obtained particles size. However, the droplets in the spray undergo inhomogeneous fluctuations as well in size and velocities especially by increasing the T_N.

3.3.4. Effect of the injection pressure P_N on the spray flash evaporation of acetone on the mean droplet size*, U and V*

The effect of the nozzle pressure P_N was investigated at 110°C for two pressures of 20 bar and 40 bar and the results are presented in **Fig.15**. It is important to notice that less measurements were collected at 20 bar that can explain the triangularization issue due to a lower concentration of acetone which disturbed measurement for the 3D representations of V. The effect of P_N is presented along the axis. A full 3D representation is shown Fig. S12.

The axial velocity is slightly affected by P_N. The mean axial velocity *U* is yet lower at 20 bar than at 40 bar even of high values (above 180 $m.s^{-1}$) were reached in both cases (Fig.15A). The main

liquid cone seems to have the same dimensions (in the analyzed zone) which suggests that no noticeable effect of the inlet pressure on the spray geometry is shown as previously suggested in Table 7. However, the radial velocity is affected by the pressure. More disturbances of the radial velocity were noticed at high P_N, especially at the tip of the nozzle as shown on the 3D graph **Fig. 15-C**. From the process point of view, an increase in the inlet pressure P_N induces an increase in the flowrate. Consequently, the amount of mass flow to evaporate is higher at larger P_N.

These experimental results sustain the spray visualization (**Fig. 7**). A deeper investigation must be carried out regarding the effect of P_N and more especially on the pressure ratio R_P. Indeed, in the operating conditions tested, the flash boiling of the solvent spray does not seem to be affected in term of mean droplet size and axial droplet velocities. The consistency in the width of the spray is in accordance with the work of Lammana *et al.* [29].

Fig.15. Effect of P_N on U, V and D_{32}

From these data, it seems that the flash boiling here is directly related to the nucleation bubble rate in accordance with literature. So, the fast depressurization induces bubble nucleation and jet disintegration through bubble bursting. In the operating conditions where the R_p is very high, the rapid expansion of the jet is so fast that the system does not relax until thermodynamic equilibrium in the two-phase flow region. The increase of pressure P_N does not affect significantly the two parameters characterizing flash boiling R_p and ΔT_{SH}. The increase of P_N will mainly change the flowrate inside from the tank to the nozzle. So, a larger amount of acetone will stay in the

crystallization reactor. R_P value are the same for both cases presented here. Shock flow is expected (R_p>50 [29]) and the maximum mass flow rate is limited by sonic condition (Chapman Jouguet). As a result, the supersonic expansion ends by shock waves to match the chamber pressure. Herein the limitations are similar which explain the same limitation obtained in terms of droplet size or maximum velocity reached. The discrepancies in flow disturbance are probably related to the amount of acetone entering the chamber compared to the exhaust capacity. P_N does not seem to be the main parameter for controlling the droplet evaporation in our case but is more related to the hydrodynamic characteristics of the droplets.

3.3.5. Comparison of droplet size and velocities in the axial position for different solvents

The nature of the solvent affects the spray characteristics. Four solvents were chosen and their physical properties are given in **Table 2.** Three of them are polar aprotic and methanol is polar protic. Their molar vaporization ratio was estimated by Simulis Thermodynamics. For same operating conditions, the vaporization is promoted in the order ethyl acetate, methyl acetate, acetone and methanol.

Fig.16 depicts the droplet size and velocities (axial or radial) distribution evolution centered to the nozzle in the Z position. Mean diameter and velocities evolution along the Z-axis are provided in the SI files (**Fig. S11**). The initial droplet size depends on physico-chemical parameters such as the viscosity and the surface tension. No significant difference is observed between the different surface tension investigated and mean droplet sizes are in the same range for all the solvent at Z=0. Further in the Z direction, larger sizes are obtained with methanol. Discrepancies are noticed

in the size distribution. Droplet size distributions are shifted to the left in case of ethyl and methyl acetate and to the smaller size when measurements are performed in the axial direction Z. The size evolution is related to the evaporation, promoting the appearance of smaller droplets. These droplets tend to disappear as a first place and the mean droplet size remains constant (balance between evaporation/bursting). The decreasing of the droplet size is more significant for the solvent presenting the highest vaporization ratio X_{vap} (**Table 6**).

The main effect on the droplet size is related on the thermal properties in particular the saturation pressure and the latent heat of vaporization. The axial droplet velocities change with these thermal properties of the fluid. The enhancement of the vaporization increases the droplet velocity due to the expansion breakup mechanism. In the same way, the axial velocity increases with the evaporation. Highest velocities are then reached for ethyl acetate and methyl acetate. As discussed earlier, the radial velocity is an indicator of the high kinetic energy zone and then provides some information on the spray flash zone.

Fig. 16. Droplet and velocities distribution for the four solvent sprays in the jet centerline (0-0-Z) for three Z position (0, -6 and -11 mm).

3.3.6. Spray study in SFE process

This part underlines the mechanism of flash evaporation in the operating conditions of the SFE process. The parameters which affects the spray and especially the droplet size and velocities are the T_N and the solvent. Both PDPA and visualization confirm the increase of turbulence and zone of high kinetic energy by increasing the superheat degree. Combining an appropriate choice of

solvent of given thermodynamic properties and T_N enables to control the evaporation. It is crucial because this parameter contributes to tune the supersaturation for crystallization.

4. Discussion: solvent spray study and particle size. How to tune particle size or morphology with the operating conditions?

4.1. Effect of the nozzle temperature T_N on the droplet and particle size

From **Fig.1**, T_N was identified as a noteworthy parameter that directly drives the process through the control of the supersaturation by managing utmost parameters: the solubility and the evaporation rate.

By studying the solvent spray, T_N affects both ΔT_{SH} and R_p. By increasing R_p the total vaporized solvent mass increases as well as the associated vapor pressure. In our case, R_p increases by changing the T_N and maintaining P_V. The on-line monitoring of the spray droplets and the visualization of the spray with high-speed camera show a short decrease of the droplet size, an increase of the droplet mean axial velocity and high radial velocity at the tip of the nozzle and at the edge of the spray. The zone at the center of the spray is a region with a high kinetic energy especially at the nozzle tip where high radial velocity V are identified. In this area, the internal energy in terms of superheat is transformed in kinetic energy by evaporation of the bulk, breakup of the jet and the very fast expansion of the resulting droplet in the vertical and horizontal directions. The phenomenon is more intense by increasing the superheat degree. Increasing the temperature acts on the R_p so on the bubble cluster generation. At a certain point, the number of critical bubble nuclei remain constraint in a confined volume whereas there is a depletion in

the available liquid volume. This could explain why the diameter remains almost constant after a certain distance from the axis in the investigated conditions. Due to volume depletion, the evolution of the spray is then mainly due to evaporation process and secondary nucleation can be prohibited. However, it is possible that the rate of vaporization is limited at high initial superheat, as in our case. Indeed, in case of shock flow, the maximum mass flux reaches a limit.

Moreover, according to **Table 6**, the vaporization ratio X_{vap} of solvent increases with T_N. A simplified calculation based on the kinetic theory of gases, as stated in the classic work of Knudsen [39], based on the work of Hertz [40] provides the evaporation mass flux according to equation Eq. 4.

$$\dot{m}_V = q_e \sqrt{\frac{M}{2\pi R}} \left(\frac{P_L(T_L)}{\sqrt{T_L}} - \frac{P_V}{\sqrt{T_C}} \right) \quad (4)$$

M is the molecular weight of the solvent, R the ideal gas constant, T_L the liquid temperature, T_C, the temperature inside the crystallization reactor, P_L is the liquid pressure and P_V the pressure of the surrounding media, the vacuum pressure.

q_e is an adjustable parameter which varies from 0 to 1. A value of 0.62 was taken according to the work of Smith *et al.* [41] and Gebauer *et al.* [37]. Values calculated are reported in **Table 8**. P_L is calculated from the Raoult's law.

Table 8: calculation of the evaporation mass flux $\dot{m}_V$ at initial condition

It suggests very short evaporation time in the range of 0.13 to 0.05 ms for solvent droplet of 10 µm and 0.005 ms to 0.01ms for solvent droplet to 1µm. Solvent droplets are then evaporated in a very short time inside the crystallization reactor. Additionally, the droplet seems to be

completely evaporated 40 mm from the nozzle tip according to Fig.7 and Fig.8 in the investigated conditions. The droplets evaporate faster by increasing T_N. As a consequence, by adding solute, the concentration increases faster inside droplet and the supersaturation is reached at a shorter time at high temperature. Depending on the induction time, the nucleation begins and is promoted at high superheat degree. More nuclei are probably generated and it explains the smallest particles size obtained in crystallization at higher T_N as detailed in section 3.1.

So, to tune particle size, it is important to master the evaporation rate. Increase the evaporation rate will lead to decrease particle size. This rate can be controlled by choosing the appropriate solvent, by changing the nozzle temperature or the vacuum pressure.

4.2. Effect of the nozzle pressure P_N on the droplet and particle size

From **Fig.1**, P_N was identified as a process parameter responsible for droplet generation and supersaturation build-up. This parameter governs the flowrate. The study of the spray shows that the pressure P_N does not affect the droplet size at a certain distance from the nozzle. The droplet velocity is yet slightly impacted. The high kinetic zones define the same volume in the chamber suggesting no real change of the flash boiling. Radial velocities are however more intense at the tip of the nozzle and spray visualization confirms the high turbulence zones.

However, the particle size in case of crystallization is significantly different depending on P_N. Indeed, it is to correlate to the exhaust of the mass flowrate. It is particularly true at high pressure and low super heat degree. The limiting mass flow rate depends on the initial injection pressure and temperature. At fixed P_N, the increase of T_N leads to higher limited mass flow rate according

to Chapman-Jouguet [42]. It explains the smaller particles obtained at higher superheat degree. In the tests performed, higher pressure P_N provides bigger particle sizes. The respective flowrate at 40 bar and 20 bar are estimated to 10.5 mL.min^{-1} and 7.5 mL.min^{-1} which corresponds to gas volume flowrate of 27 and 35 m^3.h^{-1} after evaporation.

P_N is a parameter which will be limiting because the (P_N, T_N) conditions for the fluid must be chosen to provide a superheating liquid just before the nozzle inlet. It is also related to the expected production because it controls the inlet flowrate. The limiting parameters are the **volume of the crystallization chamber and the vacuum pump** needed to remove the exhaust gases. A special attention should be paid to avoid too high pipe restriction. Too large differential pressure in pipes might be responsible for limitation of the maximum volume flow through the pipeline and prevents the gas exhaust despite of the vacuum pump capacity.

4.3. Solvent effect: Combined effect of solubility and evaporation to drive polymorphism

From **Fig.1**, solvent will be responsible for droplet generation, evaporation properties and solubility of the solute leading to supersaturation buildup. The choice of the solvent is crucial for the SFE process. The solvent must be easily vaporizable, offering high heat capacity and low enthalpy of vaporization to ensure heat transfer. At the same time, in crystallization process, the solvent is one of the parameter which affects polymorphism [43]. Indeed, primary factors are supersaturation, temperature, stirring and secondary factors are solvent, impurities or surface. The choice of the solvent results often from economic and environmental constraints, linked here to the evaporation ability.

The results presented in part 3 are reviewed regarding both evaporation of the solvent and solubility of the organic compounds. Evaporation mass flux was calculated based on Eq.4 and presented in **Table 9** as well the molar vaporization ratio.

Table 9: calculation of the evaporation mass flux m_V at initial condition

Solvents can be classified in the following order according to their evaporation mass flux: methyl acetate, acetone, ethyl acetate and methanol. The study of the solvent spray with the PDPA show that the methyl and ethyl acetate present the smallest droplet size and highest axial droplet velocity which sustain their better evaporation. To understand the particles size and morphology obtained, evaporation and solubility were concomitantly examine. In the SFE process, the supersaturation is mastered by tuning these both parameters. In the case of HMX, different polymorphs are obtained depending on the solvent used: HMX-4 presents the α-form whereas the HMX-6 is a mixture of γ and β as presented in Table 4 (see also **Fig.S4** in SI). However, the particle size distributions of both samples are almost superimposed despite the lowest solubility of HMX in methyl acetate. Compiling data on evaporation reveals that the vaporization ratio X_{vap} and evaporation parameters such as R_p and ΔT_{SH} calculated for both acetone and methyl acetate in **Table 6** exhibit similar value but the evaporation mass flux is neverthless higher in case of methyl acetate (**Table 8**). Measurements of solvent droplet size and axial velocity confirm the better evaporation ability of methyl acetate : the droplet size is slighlty lower and the axial velocity is larger than value reached for acetone (Fig. 16 and **Fig.S11**). If in both case evaporation performance are high, the solubility of HMX in acetone is 6 times higher than in methyl acetate. As a consequence, the size and morphology of particles are here mainly driven by the solubility and subsequent supersaturation. HMX displays a solubility of 2.8wt.% in acetone which drops to

0.49wt.% in methyl acetate. The degree of supersaturation therefore reaches a higher value promoting a faster nucleation in case of HMX-6. Whereas a smaller size was expected, the obtained particles are in the same range but the particle size distribution is narrower with methyl acetate. The crystallization occurring in the SFE process, like in other spray method [44], is kinetically driven and consequently produces mostly metastable phases. Metastable forms of the crystal could be obtained according to the residence time of the crystal in its solvent. In particular, at the initial stage of the crystallization, a metastable form will appeared during the transition of the saturated solution to the supersaturated solution. If the system is able to reach its thermodynamic state, the most stable form will be achieved. The next steps will be affected by the nucleation kinetics, lattice growth rate and obviously by the evaporation rate which drives the time during which the crystal is in the solvent. The most stable β form requires a longer time of the crystal in solution [45]. Herein HMX appears at early stage in methyl acetate compared to acetone due to the solubility difference which can explain the difference in polymorphism and the presence of more stable phases.

HMX-1 and HMX-5 differ again by their solvent nature. Water is an antisolvent and as a consequence HMX solubility decreases in the mixture water/acetone [13]. In the same time, molar vaporization ratio are in the same range for both solvent in this operating condition. The supersaturation degree is higher for HMX-5 than for HMX-1. Nucleation will start faster. An increase of the supersaturation leads to an increase of the nucleation rate [46]. More nuclei are generated and the high evaporation rate enables to obtain smaller particles. HMX obtained is initially in γ form but evolved in a mixture of β and γ. Herein the HMX appears at early stage in

the water/acetone compared to acetone due to the solubility difference which can again explain the difference in polymorphism.

Solvent affects also polymorphism during CL-20 crystallization by SFE. Same results were obtained for CL-20 crystallized in acetone (CL- 20- 4) and methyl acetate (CL-20-6) regarding polymorphism. The solubility of CL-20 is very high in both solvents, acetone and methyl acetate (**Table 3**) compared to the other organic compounds studied. The evaporation is not significantly improved. The supersaturation was changed by leading to similar phase and a slight decrease in particle size.

A different polymorph is obtained for CL20-7. Solubility of CL-20 is very low in methanol compared to solubility in acetone (**Table 3**). The initial supersaturation degrees at ambient temperature were respectively 0.79 and 0.01. Regarding the solvent spray study, larger droplet sizes were obtained for methanol as well as lower velocities suggesting moderate evaporation conditions compared to the other solvents. The evaporation mass flux $\dot{m}_V$ and the molar vaporization ratio X_{vap} are larger for acetone than for methanol suggesting a faster evaporation rate. So CL-20 in methanol present lower evaporation and solubility than CL-20 in acetone. At the end, particles with a high polydispersity were obtained in methanol. If supersaturation is probably reached faster and promote nucleation, the slower evaporation can be responsible for particle growth. A more stable phase is obtained with methanol probably due to the slower kinetics involved.

Supersaturation and evaporation rate will play a role on the control of the polymorphism. To master polymorphism, additional data will be mandatory including **solubility curve and**

vaporization kinetics data. **The synergy between evaporation rate and solubility will help us to master supersaturation and provide a better control of polymorphism.**

5. Conclusions and perspectives

This study is the first which combines the crystallization results and the solvent spray study.

The study of pure solvent reveals spray formation mechanism. The flash boiling phenomenon is responsible for the droplet expansion in the vacuum chamber. The spray analysis highlights the mechanisms of bubble nucleation and droplet expansion. Different process parameters were studied. The inlet temperature T_N affects the droplet size, the droplet velocities and the geometry of the spray. Indeed, it sustains the bubble nucleation leading to a fast bubble bursting. On the contrary, the injection pressure, P_N, does not directly intervene in the flash boiling process but it modifies hydrodynamics and flowrate of the spray. To go further in the understanding of the mechanisms occurring in this process, it seems a key point to investigate the effect of the injection pressure and vacuum pumping. Indeed, this parameter was not really investigated in the previous crystallization tests. In the current design of the SFE, it is of primary importance to study crystallization at moderate pressures and see the effect on the droplet atomization and particle size.

Compelling data solvent spray and crystallization give first insights on the mechanism involved in the spray flash evaporation. The main limitation relies on the solvent which is concomitantly the bounding parameters for the solubility and for the evaporation rate. The

particle size is directly affected by the evaporation rate, all the parameters being constant. The effect of the solvent on the polymorphism demonstrates the interest of the study of spray evaporation. However, this study must be supplemented with solubility measurement in a wide range of temperature to master the supersaturation. It is necessary to go deeper in the study to establish supersaturation curves. The polymorphism is controlled in part by supersaturation and therefore by the solvent evaporation kinetic, as a primary factor. Obviously other parameters could be studied such as additives or host-guest composition as secondary factors affecting polymorphism.

The tuning of particle size and morphology in the SFE process for a solute/solvent system will depend on the evaporation conditions and the management of the supersaturation during the process. The development of this set-up provide knowledge on the evaporation and the next step will be to study the concentration effect and correlate data with solubility.

References

[1] B. Risse, Continuous crystallization of ultra-fine energetic particles by the Flash-Evaporation Process, 2012.

[2] D. Spitzer, B. Risse, F. Schnell, V. Pichot, M. Klaumünzer, M.R. Schaefer, Continuous engineering of nano-cocrystals for medical and energetic applications, Sci. Rep. 4 (2014). https://doi.org/10.1038/srep06575.

[3] M. Klaumünzer, L. Schlur, F. Schnell, D. Spitzer, Continuous Crystallization of ZnO Nanoparticles by Spray Flash Evaporation vs. Batch Synthesis, Chemical Engineering & Technology. 38 (2015) 1477 1484. https://doi.org/10.1002/ceat.201500053.

[4] A. Sève, V. Pichot, F. Schnell, D. Spitzer, Trinitrotoluene Nanostructuring by Spray Flash Evaporation Process, Propellants, Explosives, Pyrotechnics. 42 (2017) 1051–1056. https://doi.org/10.1002/prep.201700024.

[5] J.-E. Berthe, F. Schnell, Y. Boehrer, D. Spitzer, Nanocrystallisation of Ammonium DiNitramide (ADN) by Spray Flash Evaporation (SFE), Propellants, Explosives, Pyrotechnics. 43 (2018) 609–615. https://doi.org/10.1002/prep.201800039.

[6] B. Risse, D. Hassler, D. Spitzer, Preparation of nanoparticles by flash evaporation, WO2013117671 A1, 2013.
[7] B. Risse, D. Spitzer, Cristallisation de nano-cocristaux par Spray Evaporation Flash (SFE), n.d.
[8] B. Risse, D. Spitzer, D. Hassler, F. Schnell, M. Comet, V. Pichot, H. Muhr, Continuous formation of submicron energetic particles by the flash-evaporation technique, Chemical Engineering Journal. 203 (2012) 158 – 165. https://doi.org/http://dx.doi.org/10.1016/j.cej.2012.07.032.
[9] F. Pessina, F. Schnell, D. Spitzer, Tunable continuous production of RDX from microns to nanoscale using polymeric additives, Chemical Engineering Journal. 291 (2016) 12–19. https://doi.org/10.1016/j.cej.2016.01.083.
[10] W. Zeng, M. Xu, G. Zhang, Y. Zhang, D.J. Cleary, Atomization and vaporization for flash-boiling multi-hole sprays with alcohol fuels, Fuel. 95 (2012) 287 – 297. https://doi.org/https://doi.org/10.1016/j.fuel.2011.08.048.
[11] M.E. Sitzmann, S. Foti, C.C. Misener, Solubilities of High Explosives: Removal of High Explosive Fillers from Munitions by Chemical Dissolution, DTIC Document, 1973. http://oai.dtic.mil/oai/oai?verb=getRecord&metadataPrefix=html&identifier=AD0773078 (accessed July 22, 2015).
[12] D.-Y. Kim, K.-J. Kim, Solubility of Cyclotrimethylenetrinitramine (RDX) in Binary Solvent Mixtures, J. Chem. Eng. Data. 52 (2007) 1946–1949. https://doi.org/10.1021/je7002463.
[13] L.-Z. Chen, J. Zhang, W.-Y. Wang, Y. Diao, Solubility of β-HMX in Acetone + Water Mixed Solvent Systems at Temperatures from 293.15 K to 313.15 K, Journal of Solution Chemistry. 41 (2012) 1265–1270. https://doi.org/10.1007/s10953-012-9872-x.
[14] E. von Holtz, D. Ornellas, M.F. Foltz, J.E. Clarkson, The Solubility of ϵ-CL-20 in Selected Materials, Propellants, Explosives, Pyrotechnics. 19 (1994) 206–212. https://doi.org/10.1002/prep.19940190410.
[15] P. Lv, H. Wang, Y. Tong, L. Dang, C. Sun, S.-P. Pang, Measurement and Correlation of the Solubility of ε-CL-20 in 12 Organic Solvents at Temperatures Ranging from 278.15 to 318.15 K, J. Chem. Eng. Data. 62 (2017) 961–966. https://doi.org/10.1021/acs.jced.6b00761.
[16] E. Limpert, W.A. Stahel, M. Abbt, Log-normal Distributions across the Sciences: Keys and Clues, BioScience. 51 (2001) 341–352. https://doi.org/10.1641/0006-3568(2001)051[0341:LNDATS]2.0.CO;2.
[17] O. Miyatake, K. Murakami, Y. Kawata, T. Fujii, Fundamental Experiments of Flash Evaporation, Bulletin of the Society of Sea Water Science, Japan. 26 (1972) 189–198. https://doi.org/10.11457/swsj1965.26.189.
[18] O. Miyatake, T. Tomimura, Y. Ide, T. Fujii, An experimental study of spray flash evaporation, Desalination. 36 (1981) 113–128. https://doi.org/10.1016/S0011-9164(00)88635-X.
[19] O. Miyatake, T. Tomimura, Y. Ide, M. Yuda, T. Fujii, Effect of liquid temperature on spray flash evaporation, Desalination. 37 (1981) 351–366. https://doi.org/10.1016/S0011-9164(00)88658-0.
[20] O. Miyatake, Y. Koito, K. Tagawa, Y. Maruta, Transient characteristics and performance of a novel desalination system based on heat storage and spray flashing, Desalination. 137 (2001) 157–166. https://doi.org/10.1016/S0011-9164(01)00214-4.
[21] R.J. Peterson, S.S. Grewal, M.M. El-Wakil, Investigations of liquid flashing and evaporation due to sudden depressurization, International Journal of Heat and Mass Transfer. 27 (1984) 301–310. https://doi.org/10.1016/0017-9310(84)90220-5.
[22] R. Brown, J.L. York, Sprays formed by flashing liquid jets, AIChE Journal. 8 (1962) 149–153. https://doi.org/10.1002/aic.690080204.
[23] S.Y. Park, B.S. Lee, An experimental investigation of the flash atomization mechanism, Atomization Spray. 4 (1994) 159–179.

[24] W. Kim, T. Yu, W. Yoon, Atomization characteristics of emulsified fuel oil by instant emulsification, J. Mech. Sci. Technol. 26 (2012) 1781–1791.
[25] H. Kamoun, G. Lamanna, B. Weigand, High-Speed Shadowgraphy Investigations of Superheated Liquid Jet Atomisation, ILASS-Americas 22nd Annual Conference on Liquid Atomization and Spray Systems. (2010).
[26] D. Yildiz, P. Rambaud, J. van Beeck, J.-M. Buchlin, Characterization of Superheated Liquid Jet Atomisation With Phase Doppler Anemometer (PDA) and High-Speed Imaging, (2006) 921–930. https://doi.org/10.1115/FEDSM2006-98255.
[27] X.X. Lu, L. Li, K.H. Luo, X.B. Ren, Y. Liu, X.F. Yan, Investigation on the Dispersal Characteristics of Liquid Breakup in Vacuum, Journal of Thermophysics and Heat Transfer. 30 (2015) 410–417. https://doi.org/10.2514/1.T4665.
[28] J.R. Simoes-Moreira, M.M. Vieira, E. Angelo, Highly Expanded Flashing Liquid Jets, Journal of Thermophysics and Heat Transfer. 16 (2002) 415–424. https://doi.org/10.2514/2.6695.
[29] G. Lamanna, H. Kamoun, B. Weigand, J. Steelant, Towards a unified treatment of fully flashing sprays, International Journal of Multiphase Flow. 58 (2014) 168–184. https://doi.org/10.1016/j.ijmultiphaseflow.2013.08.010.
[30] Handbook of atomization and sprays - Theory and application, Springer US, Ashgriz, Nasser, 2011.
[31] R.D. Oza, On the Mechanism of Flashing Injection of Initially Subcooled Fuels, Journal of Fluids Engineering. 106 (1984) 105–109. https://doi.org/10.1115/1.3242383.
[32] M. Razzaghi, Droplet size estimation of two-phase flashing jets, Nucl. Eng. Des. 114 (1989) 115–124. https://doi.org/10.1016/0029-5493(89)90130-1.
[33] Y. Kitamura, H. Morimitsu, T. Takahashi, Critical superheat for flashing of superheated liquid jets, Ind. Eng. Chem. Fund. 25 (1986) 206–211. https://doi.org/10.1021/i100022a005.
[34] V. Cleary, P. Bowen, H. Witlox, Flashing liquid jets and two-phase droplet dispersion: I. Experiments for derivation of droplet atomisation correlations, Journal of Hazardous Materials. 142 (2007) 786–796. https://doi.org/10.1016/j.jhazmat.2006.06.125.
[35] A. Günther, K.-E. Wirth, Evaporation phenomena in superheated atomization and its impact on the generated spray, International Journal of Heat and Mass Transfer. 64 (2013) 952–965. https://doi.org/10.1016/j.ijheatmasstransfer.2013.05.034.
[36] J. Gebauer, M. Kind, Experimental screening method for flash-crystallization, Chemical Engineering Science. 133 (2015) 75 – 81. https://doi.org/http://dx.doi.org/10.1016/j.ces.2014.12.034.
[37] J. Gebauer, M. Kind, Profiles of temperature, concentration and supersaturation within atomized droplets during flash-crystallization, Chemical Engineering and Processing: Process Intensification. 91 (2015) 130 – 140. https://doi.org/http://dx.doi.org/10.1016/j.cep.2015.03.012.
[38] H. Guo, Y. Li, B. Wang, H. Zhang, H. Xu, Numerical investigation on flashing jet behaviors of single-hole GDI injector, International Journal of Heat and Mass Transfer. 130 (2019) 50–59. https://doi.org/10.1016/j.ijheatmasstransfer.2018.10.088.
[39] M. Knudsen, Die maximale Verdampfungsgeschwindigkeit des Quecksilbers, Annalen Der Physik. 352 (1915) 697–708. https://doi.org/10.1002/andp.19153521306.
[40] H. Hertz, Ueber die Verdunstung der Flüssigkeiten, insbesondere des Quecksilbers, im luftleeren Raume, Annalen Der Physik. 253 (1882) 177–193. https://doi.org/10.1002/andp.18822531002.
[41] J.D. Smith, C.D. Cappa, W.S. Drisdell, R.C. Cohen, R.J. Saykally, Raman Thermometry Measurements of Free Evaporation from Liquid Water Droplets, J. Am. Chem. Soc. 128 (2006) 12892–12898. https://doi.org/10.1021/ja063579v.
[42] M.M. Vieira, J.R. Simoes-Moreira, Low-pressure flashing mechanisms in iso-octane liquid jets, J. Fluid Mech. 572 (2007) 121–144.

[43] M. Kitamura, Controlling factor of polymorphism in crystallization process, Journal of Crystal Growth. 237–239, Part 3 (2002) 2205 – 2214. https://doi.org/http://dx.doi.org/10.1016/S0022-0248(01)02277-1.
[44] H. Singh, N. Jahagirdar, S. Banerjee, Sonochemically assisted synthesis of nano HMX, Defence Technology. 15 (2019) 837 – 843. https://doi.org/https://doi.org/10.1016/j.dt.2019.04.010.
[45] M. Ghosh, S. Banerjee, M.A. Shafeeuulla Khan, N. Sikder, A.K. Sikder, Understanding metastable phase transformation during crystallization of RDX, HMX and CL-20: experimental and DFT studies, Phys. Chem. Chem. Phys. 18 (2016) 23554–23571. https://doi.org/10.1039/C6CP02185A.
[46] J.W. Mullin, ed., References, in: Crystallization (Fourth Edition), Fourth Edition, Butterworth-Heinemann, Oxford, 2001: pp. 536 – 575. http://www.sciencedirect.com/science/article/pii/B9780750648332500139.

Acknowledgment

Emeline Lobry would like to thank the University of Strasbourg and ISL for the grant funding this project. The authors would like to thank Jean Urban for his technical support and help for the 3D axis table and the workshop of the ISL for all the equipments. The authors thank also Fabien Schnell for the SEM pictures and Yannick Boehrer for the high-speed camera recording.

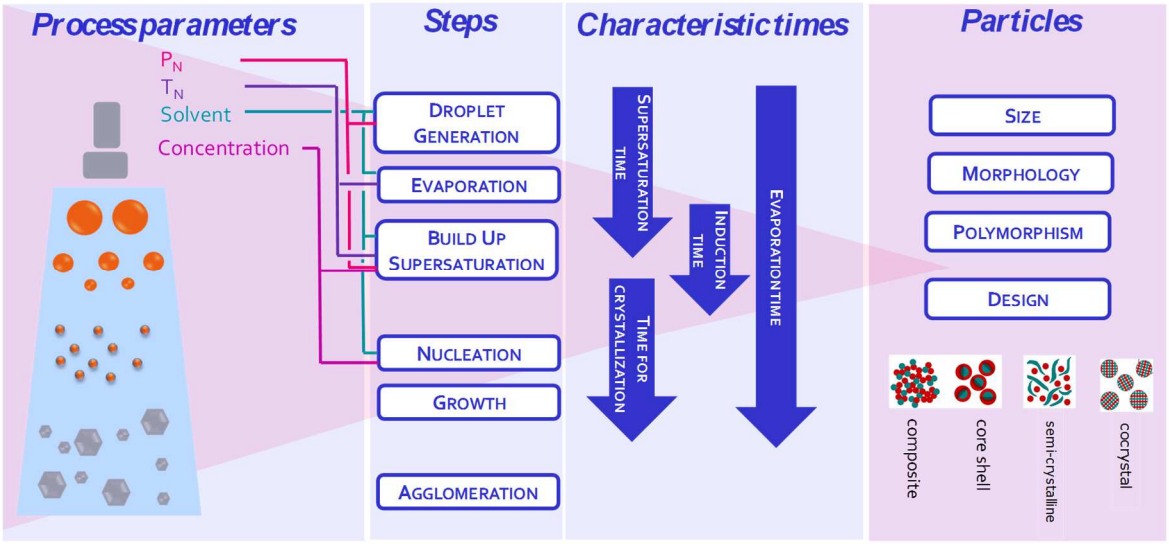

Fig. 1: Various particle morphologies prepared by Spray Flash Evaporation.

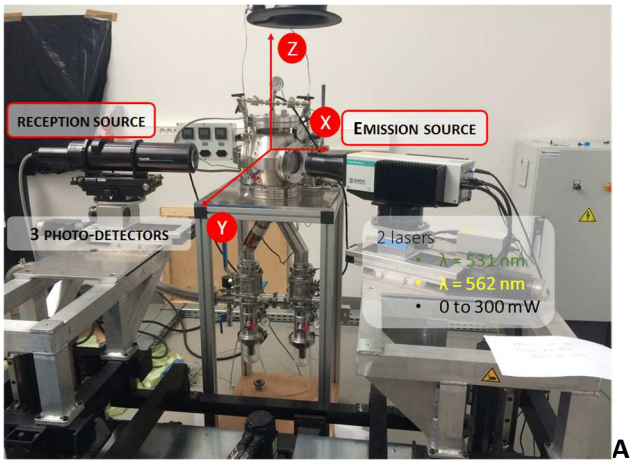

A

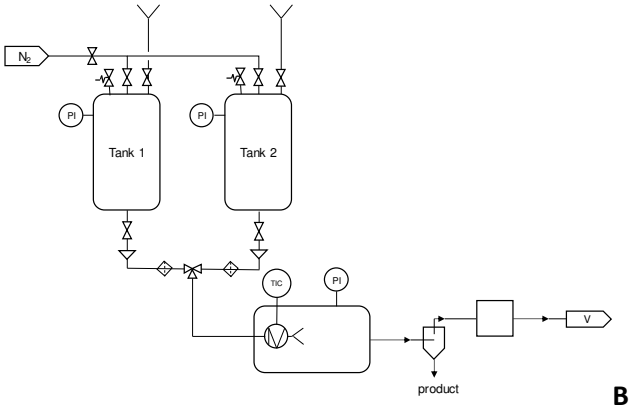

B

Fig.2. **A)** Experimental set-up, **B)** schematic representation of the experimental set-up

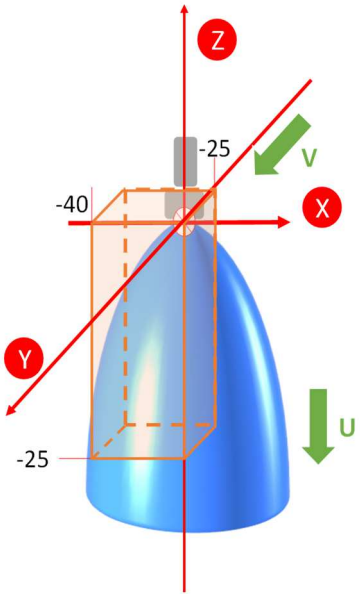

Fig. 3. Spray representation with the measurement zone depending on the XYZ axis set by the 3D axes table *(the origin is set at the nozzle outlet position and dimensions are in mm)*

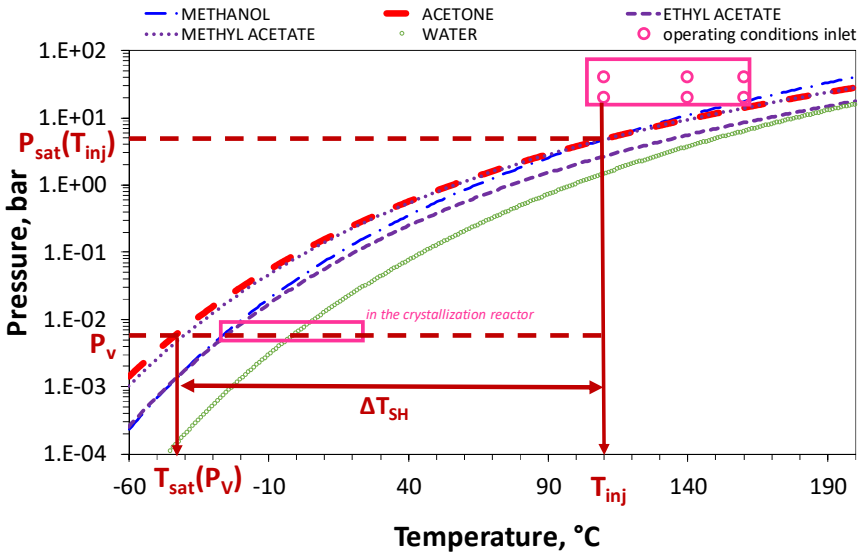

Fig.4. Saturation curves for different common solvents

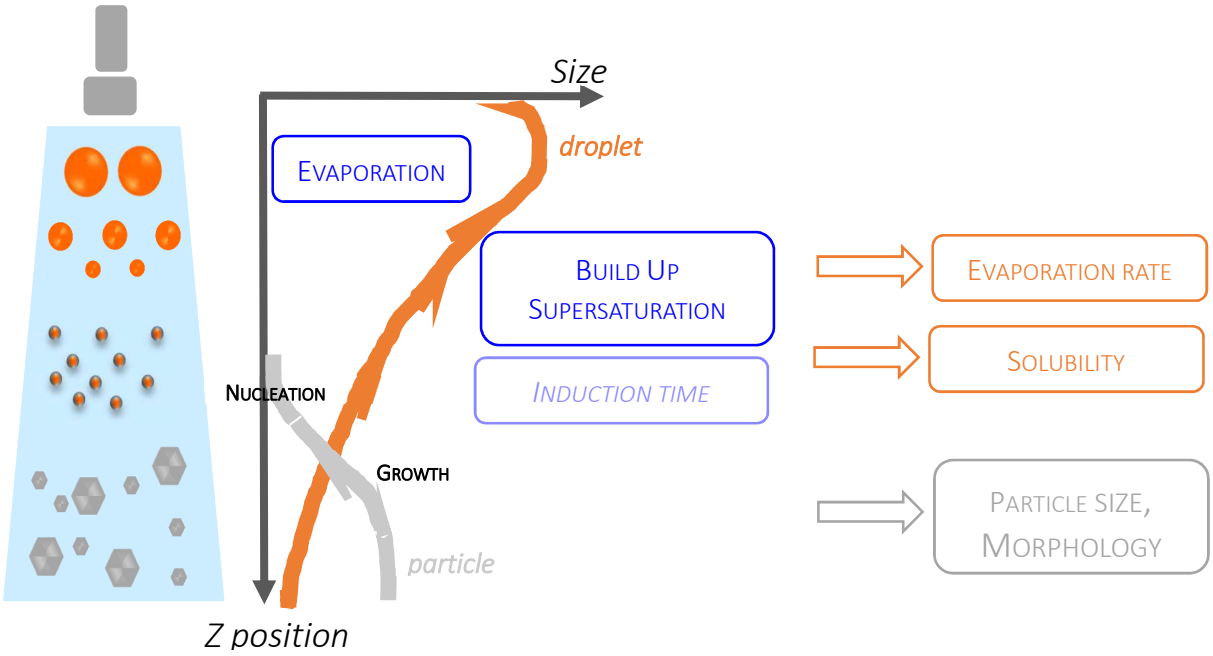

Fig. 5: Schematic representation of the SFE crystallization process – first understanding stage: from droplet evaporation to the final particle

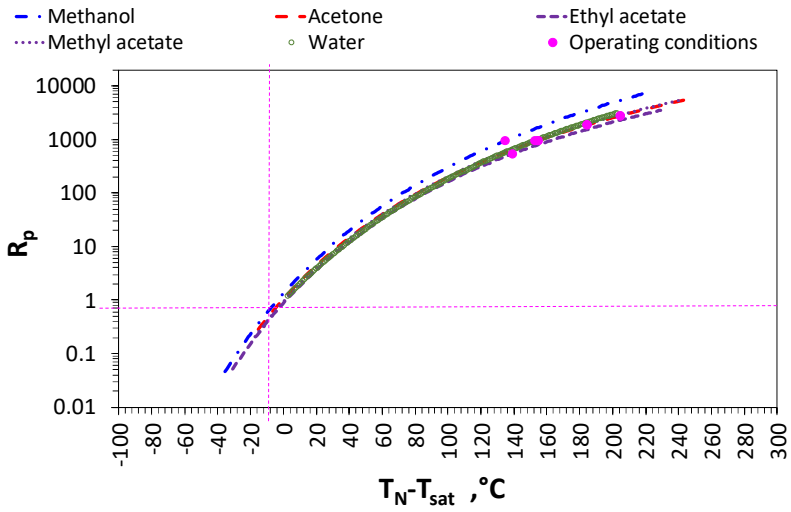
Methanol
Acetone
Ethyl acetate
Methyl acetate
Water
Operating conditions
10000
1000
100
10
1
0.1
0.01
R_p
-100
-80
-60
-40
-20
0
20
40
60
80
100
120
140
160
180
200
220
240
260
280
300
T_N-T_{sat} ,°C

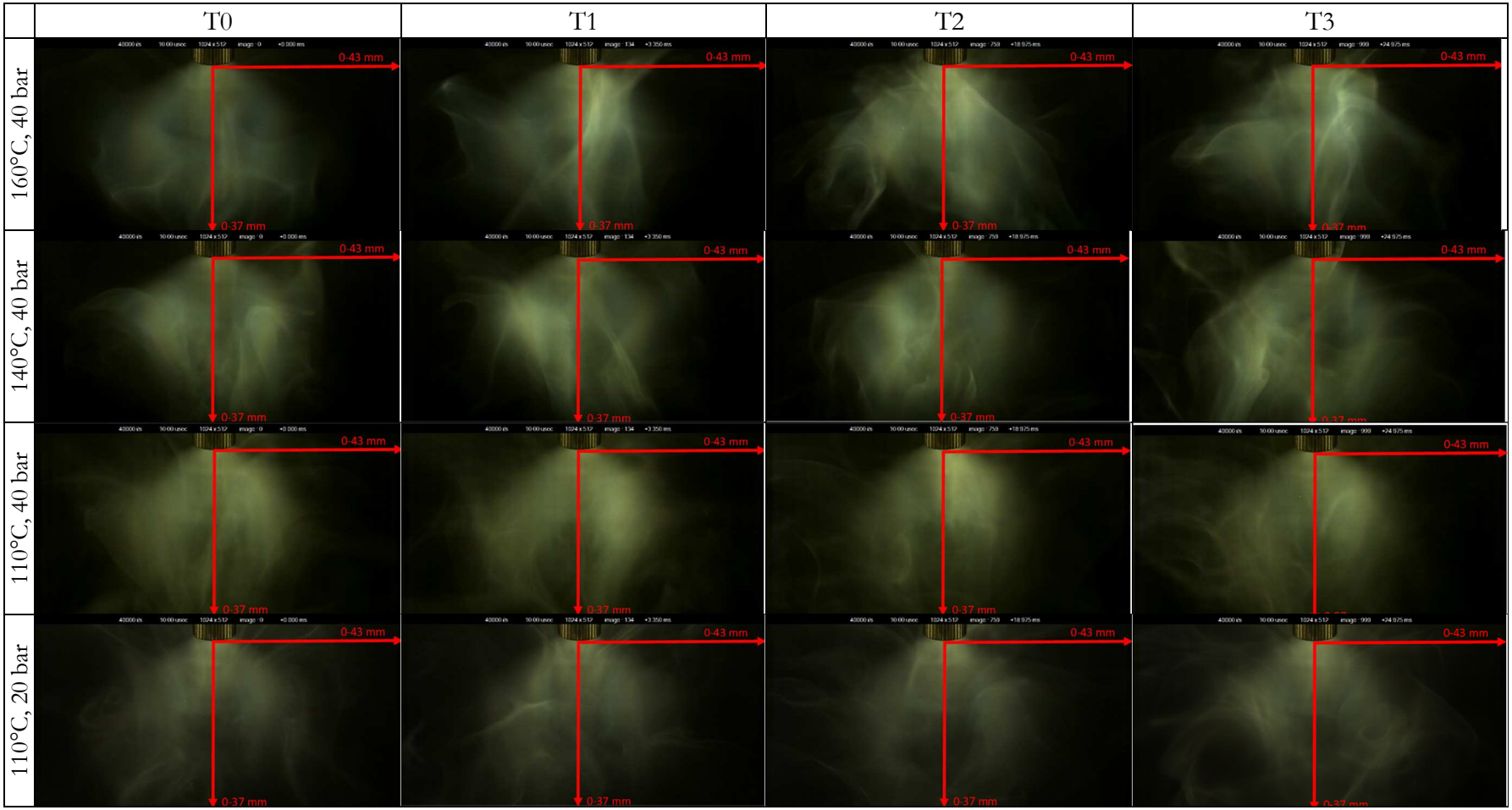

Fig. 7. Acetone spray under different operating conditions at T0, T1 (3350ms), T2 (18975ms) et T3 (74975ms)

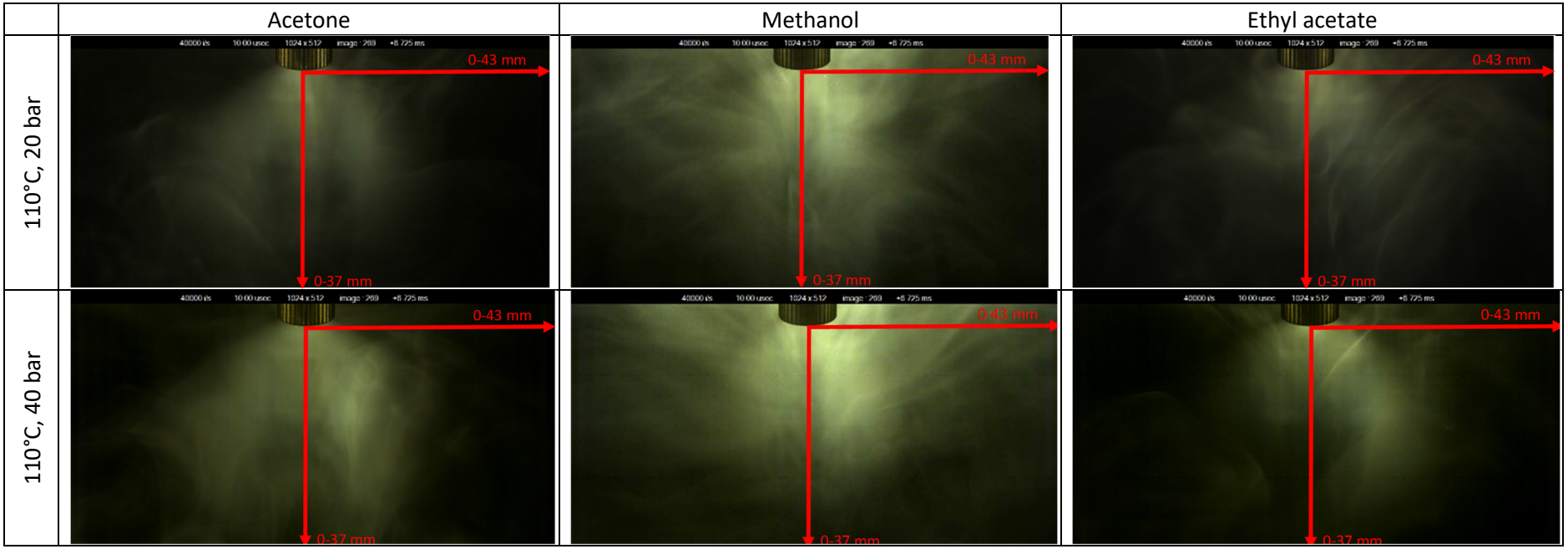

Fig. 8. Visualization of the spray for different solvents and operating conditions

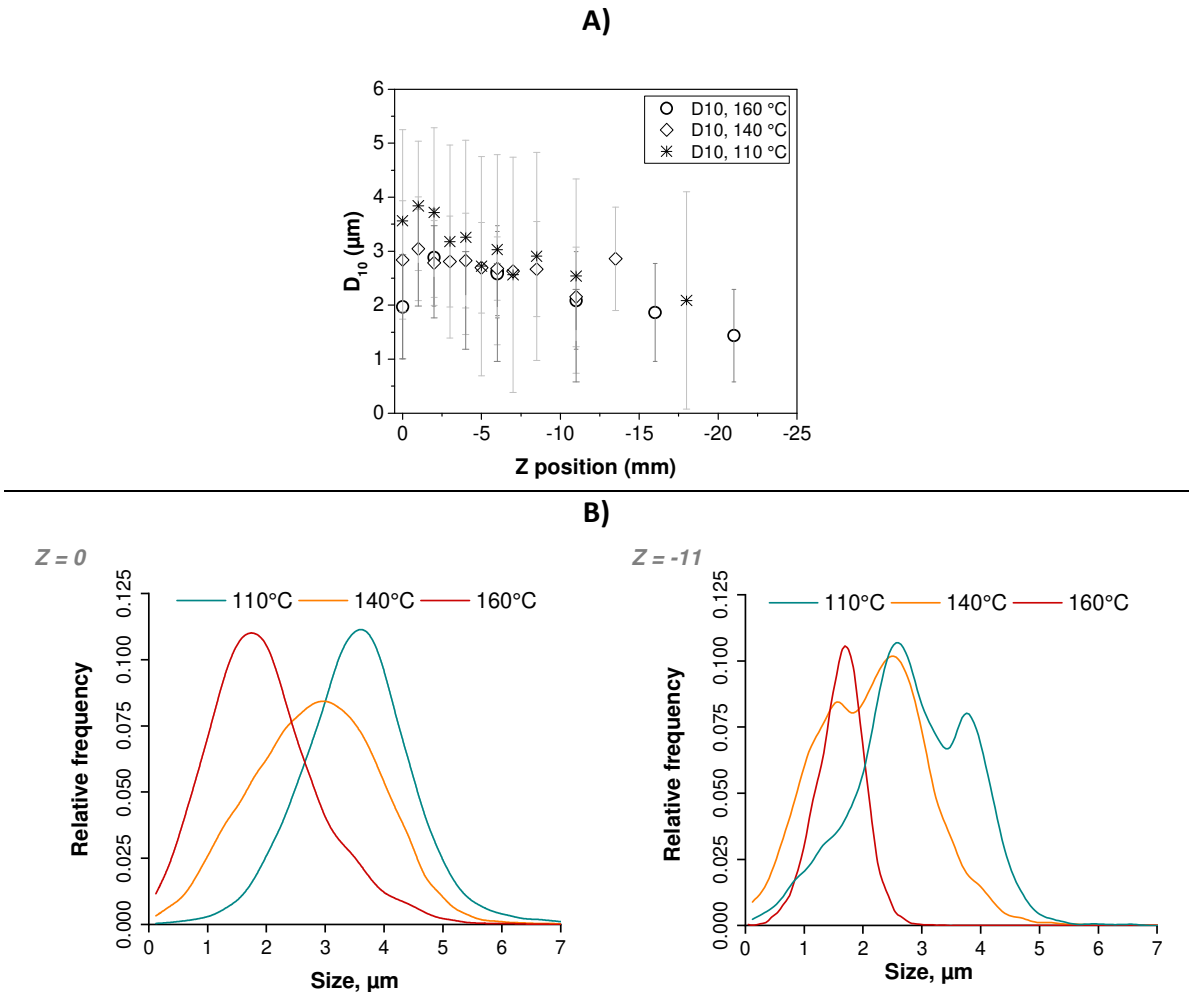

Fig.9. A) Evolution of the *D10* depending on T_N along the Z-axis at the center of the spray (X = 0, Y = 0) B) DSD depending on the temperature at 0-0-0 and 0-0-(-11).

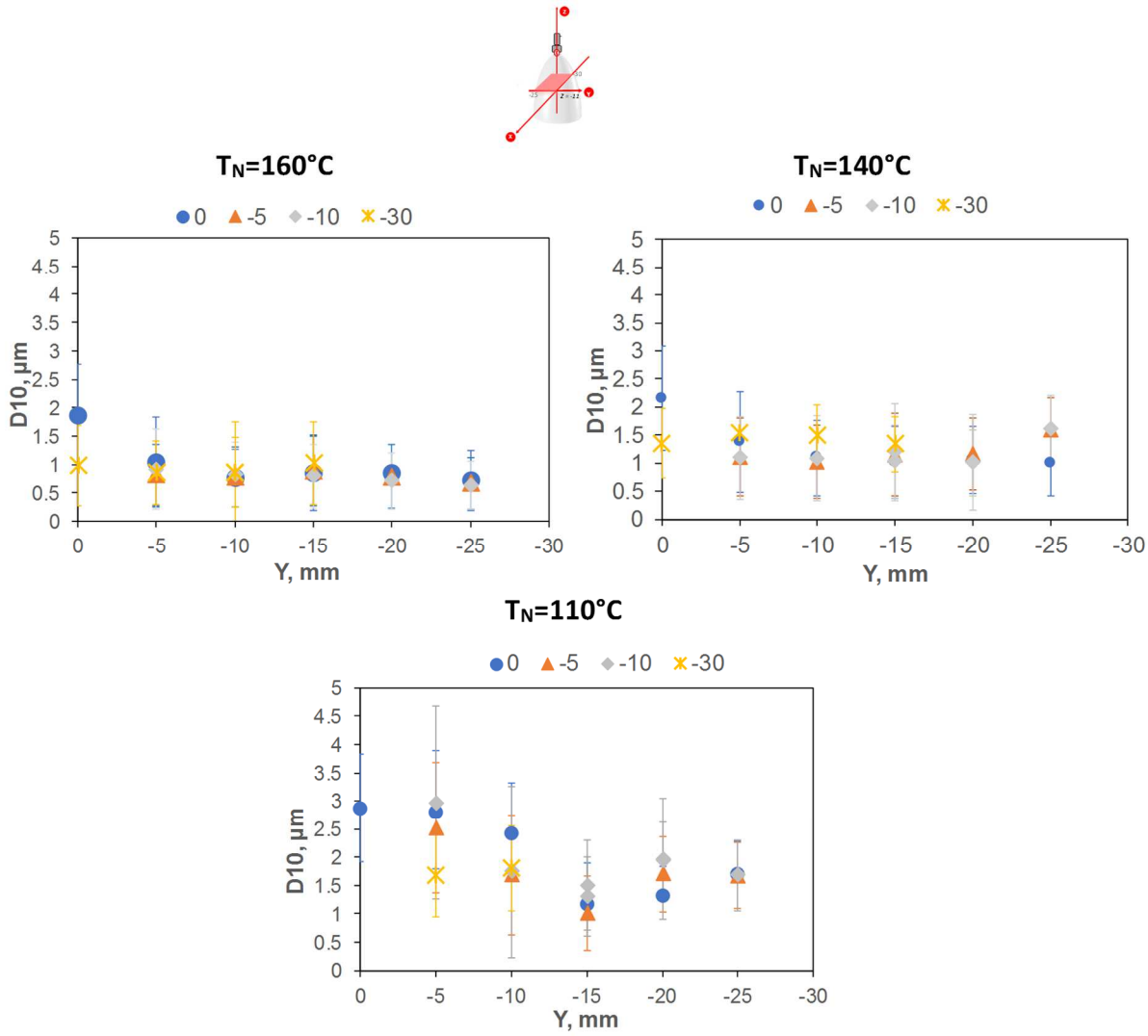

Fig.10. Evolution of the D10 at Z =-11mm in the radial direction for different X.

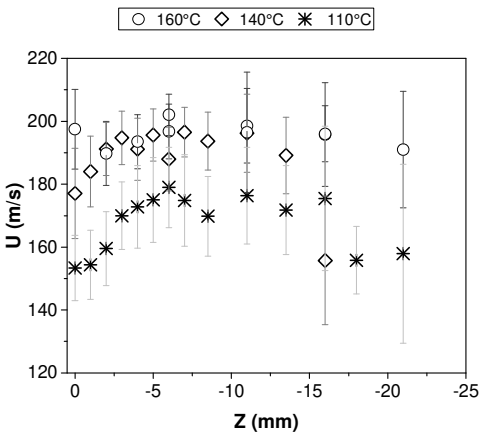

Fig. 11. Mean axial velocity *U* along the Z axis in the 0-0-Z position.

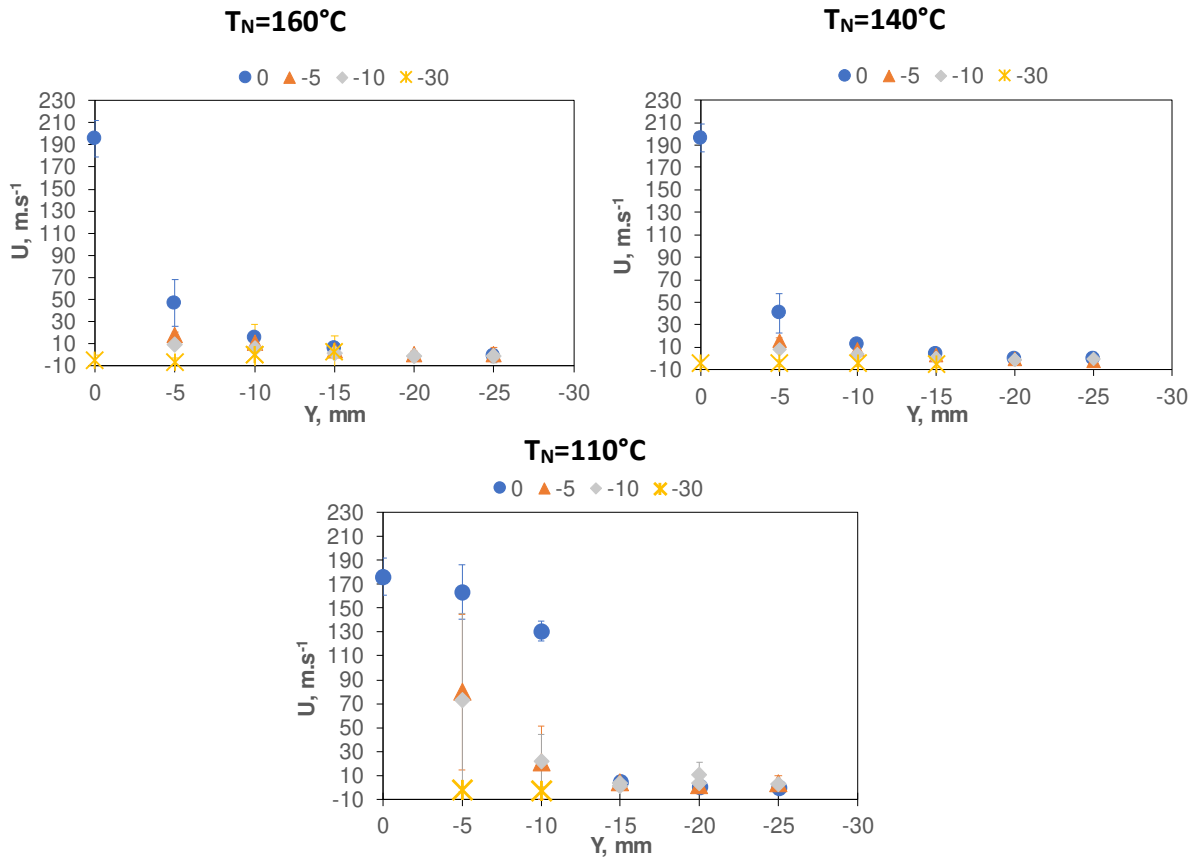

Fig.12. Mean axial velocity U at Z =-11 for the different T_N for the acetone spray at 40 bar depending on the radial position Y and for different X.

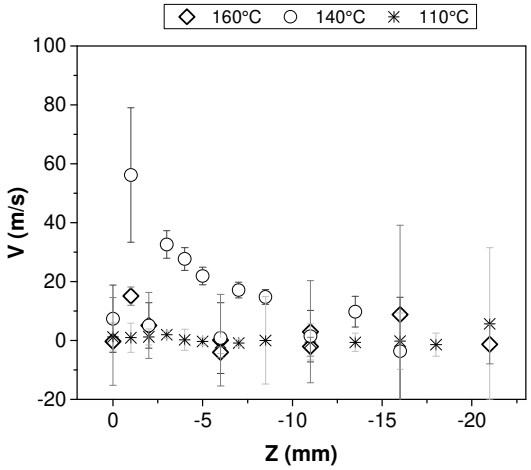

Fig. 13. Mean radial velocity *V* along the Z axis in the 0-0-Z position.

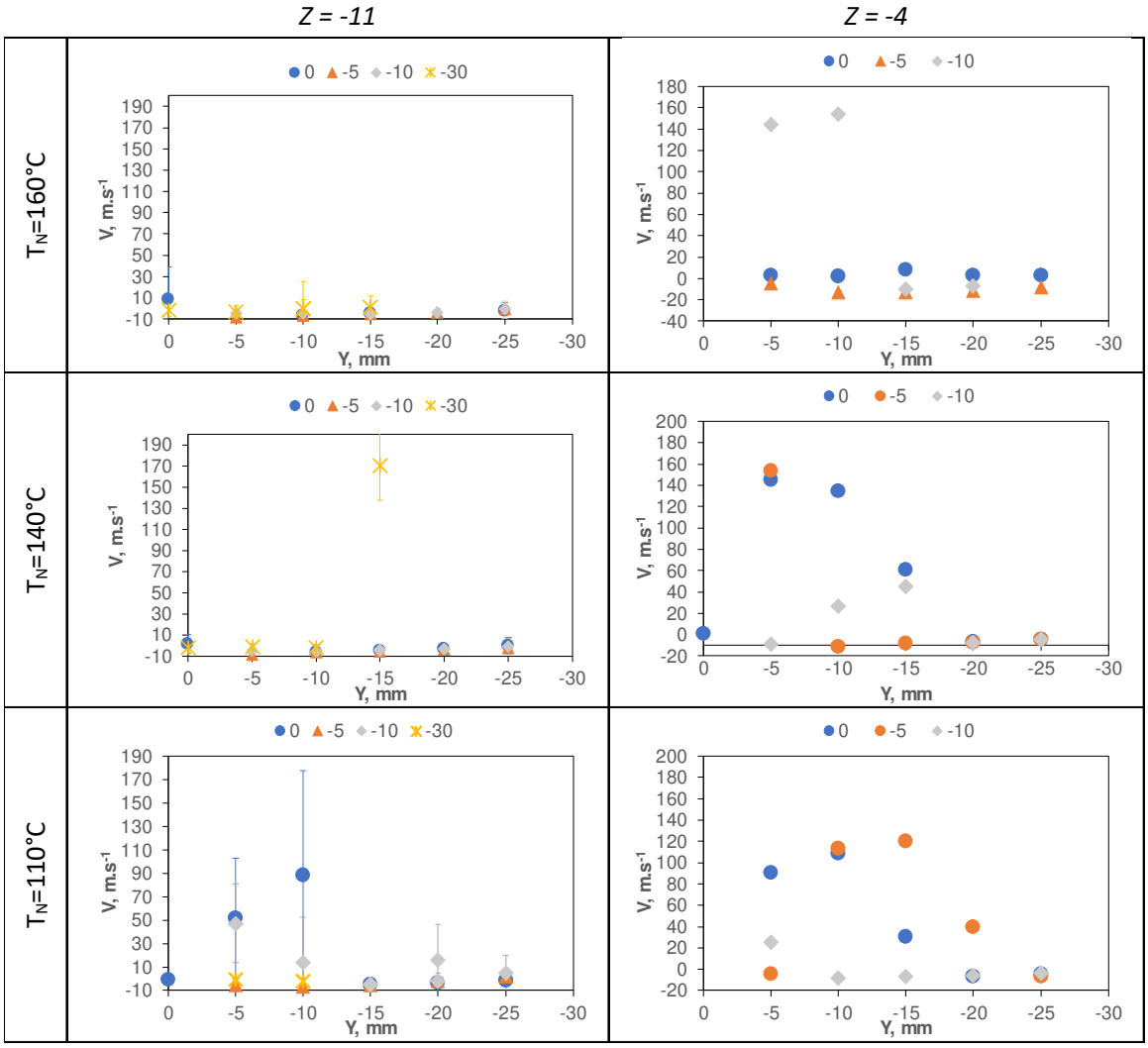

Fig.14. Effect of T_N on the radial velocity V for different positions at Z=-11mm (left) and Z = -4mm (right)

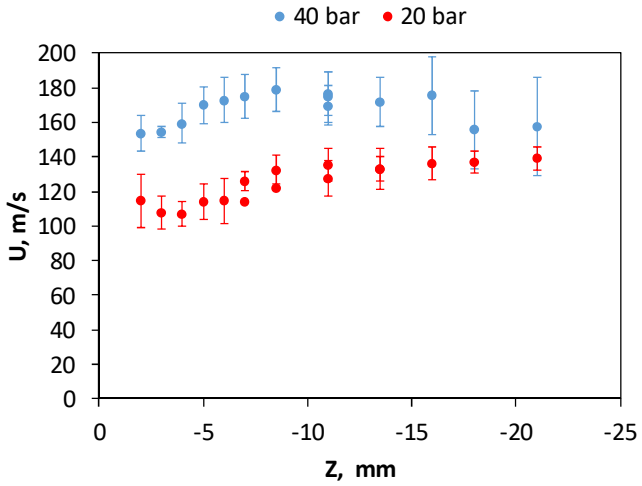

A) Axial velocity U in the center of the jet at different Z position

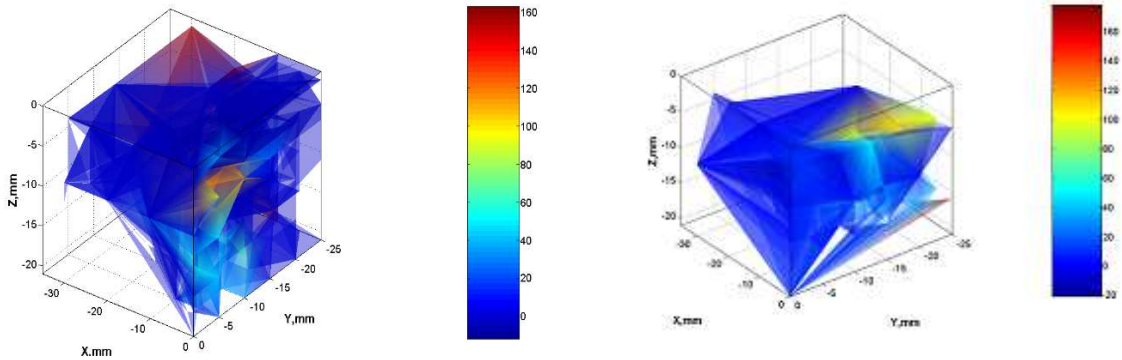

P_N=40 bar **P_N=20 bar**

B) Radial velocity V in the 3D axis

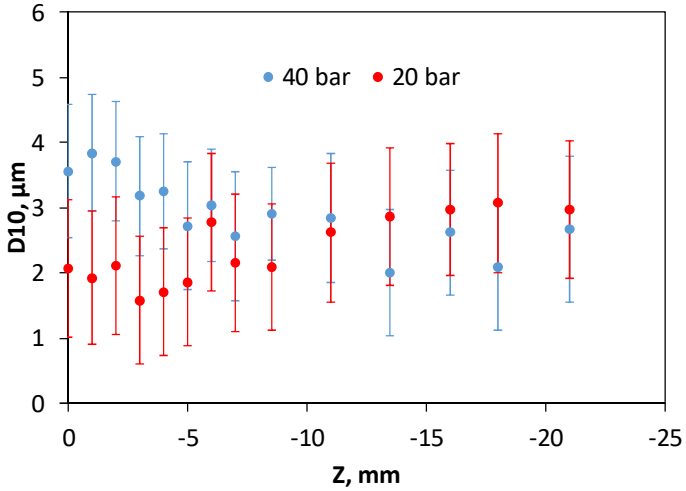

C) Mean diameter at 0-0-Z

Fig.15. Effect of P_N on U, V and D_{32}

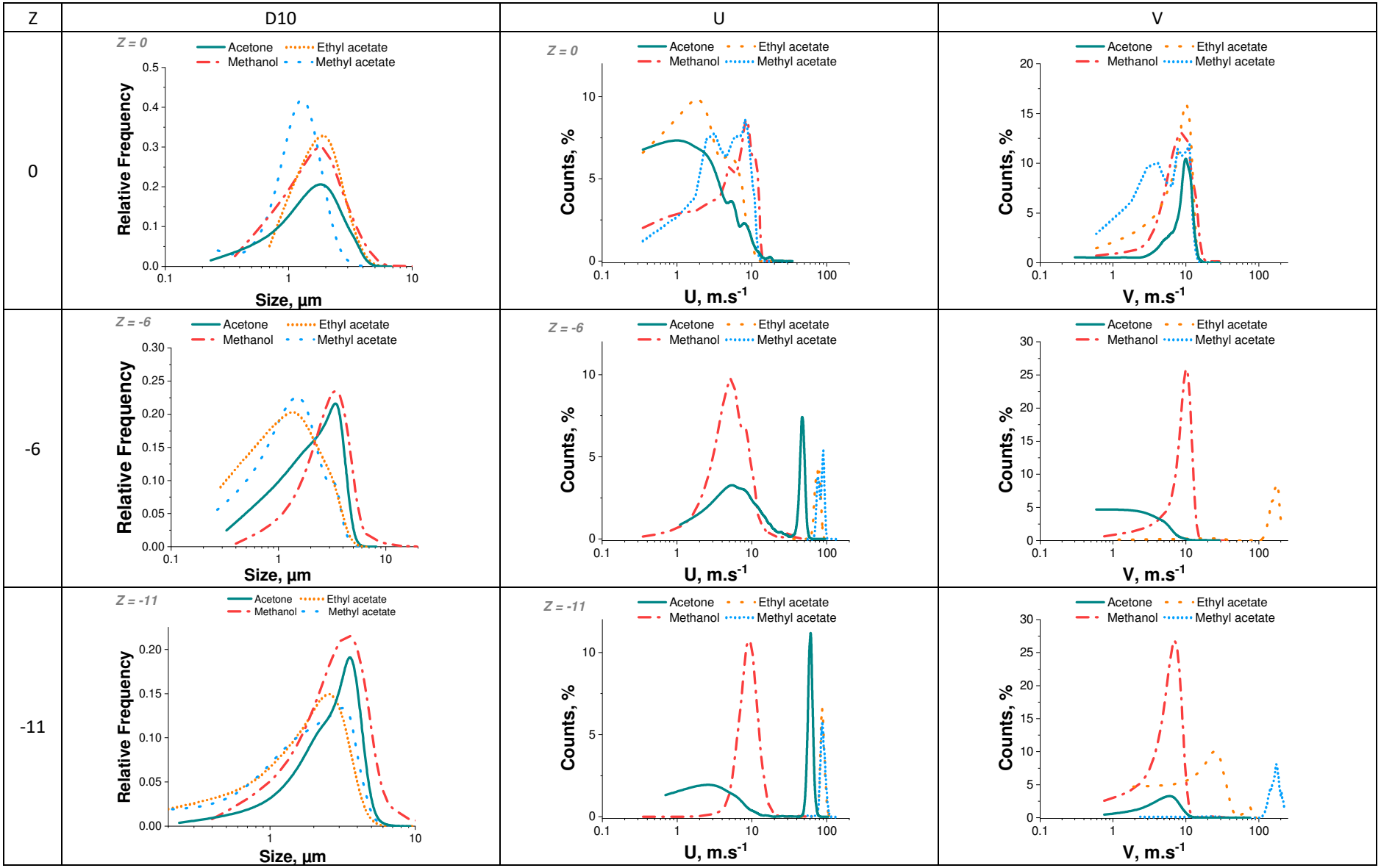

Fig. 16. Droplet and velocities distribution for the four solvent sprays in the jet centerline (0-0-Z) for three Z position (0, -6 et -11 mm).

Solvent	ACETONE	METHANOL	ETHYL ACETATE	METHYL ACETATE
Surface tension (mN.m^{-1}, 25°C)	23.04	22.2	23.2	24.5
Viscosity (mPa.s, 25°C)	0.307	0.538	0.430	0.363
Density (kg.m^{-3}, 25°C)	786.6	789.6	893.6	928.0
Critical pressure P_C (bar)	47	80.8	38.8	47.5
Critical temperature T_C (°C)	235	239.4	250	233.4

Table 1. Physical properties of different solvents.

Solvent	**T_N, °C**	**P_N, bar**	**Measurement**
Acetone	160	40	¼ of the spray
		20	
	140	40	
		20	
	110	40	
		20	
Methanol	160	40	Axial position jet centerline 0-0-Z
Methyl acetate	110	20	
Ethyl acetate			

Table 2. Operating conditions for the solvent spray tests.

Explosive	**Solvent**	**Solubility (@25°C)**	**Concentration g/100mL**	**T_N °C**	**P_N,bar**	**Sample name**
RDX	Acetone	8.2 wt.%[11]	1	160	40	RDX-1
					20	RDX-2
				110	40	RDX-3
					20	RDX-4
	Acetone/Water (90/10 %vol.)	4.89 wt.%@20°C 6.14 wt.% @30°C [12]		160	40	RDX-5
HMX	Acetone	2.8 wt.% [11]	0.3	160	40	HMX-1
					20	HMX-2
				110	40	HMX-3
					20	HMX-4
	Acetone/water	1.73 wt.% [13]		160	40	HMX-5
	Methyl acetate	0.49 wt.%		110	20	HMX-6
CL-20	Acetone	94.6 wt.% [14]	1	160	40	CL-20-1
					20	CL-20-2
				110	40	CL-20-3
					20	CL-20-4
	Methanol	2.57 wt.%[15]	0.5	160	40	CL-20-7
	Methyl acetate	>53.6 wt%[14]	1	110	20	CL-20-6

Table 3. Operating conditions for the recrystallization of different explosives (P_V=5 mbar, nozzle 80 μm).

Solute	Solvent	T_N °C	P_N bar	Sample	μ, μm	σ_d, μm	PI	Morphology	Polymorph
RDX	Acetone	160	40	RDX-1	0.65	0.34	0.52	spherical	α
			20	RDX-2	0.54	0.22	0.41		α
		110	40	RDX-3	0.67	0.30	0.45		α
			20	RDX-4	0.50	0.28	0.56		α
	Acetone/Water (90/10 %vol.)	160	40	RDX-5	0.64	0.29	0.45		α
HMX	Acetone	160	40	HMX-1	length : 3.31 width : 0.86	1.42 0.39	0.43 0.45	rod	α
			20	HMX-2	0.13	0.07	0.54	plate	α
		110	40	HMX-3	length : 2.67 width : 1.35	1.13 0.53	0.42 0.39	rod	α
			20	HMX-4	0.34	0.28	0.82	spherical	γ + α
	Acetone/water	160	40	HMX-5	0.18	0.07	0.39	spherical	γ + β
	Methyl acetate	110	20	HMX-6	0.32	0.22	0.69	sphérical	γ + α + β
CL-20	Acetone	160	40	CL-20-1	0.62	0.32	0.52	spherical	β
			20	CL-20-2	0.34	0.20	0.59	spherical	β
		110	40	CL-20-3	-	-	-	spherical	α + β
			20	CL-20-4	0.49	0.28	0.57	spherical	β
	Methanol	160	40	CL-20-7	1.89	2.37	1.25	polyhedral	α
	Methyl acetate	110	20	CL-20-6	0.46	0.29	0.63	spherical	β

Table 4: Particle size and morphology of the different explosives obtained by SFE

References	Nozzle pressure, bar	Nozzle temperature,°C	Discharge pressure, bar	Fluids
[16]	8 to 21	140	1	Water, Freon-11
[19]	10	30-147	0.02-0.4	Acetone, Ethanol, Iso-octane
[12]	1	40-80	1	Water
[21]	1	2-50	0.05 to 0.15 mbar	Water, Diglycol, Glycerol
[28]	2-5	76.5-162	0.001 – 1 mbar	Iso-octane
[26]	1-80	34.85-154 ;85	0.005-0.4	Acetone, Ethanol, Isooctane

Table 5. Different studies of spray flash evaporation in literature and their operating conditions.

	P_N	T_N	P_V	P_{sat}	T_{sat}	X_{vap}	R_p	T_N-T_{sat}
	bar	*°C*	*bar*	*bar*	*°C*			*°C*
ACETONE	20	110	0.005	4.8	-44.7	0.55	958	154.7
		140		9.4	-44.7	0.68	1882	184.7
		160		14.0	-44.7	0.78	2795	204.7
	40	110		4.8	-44.7	0.55	958	154.7
		140		9.4	-44.7	0.68	1882	184.7
		160		14.0	-44.7	0.78	2795	204.7
METHANOL	20	110		4.8	-24.8	0.36	956	134.8
ETHYL ACETATE				2.7	-29	0.63	536	139.0
METHYL ACETATE				4.8	-42.9	0.59	956	152.9
WATER/ACETONE (10/90% IN VOLUME)	40	160	0.005	14.2	-32.1	0.72	2840	192.1

Table 6. Calculation of the relevant parameters in the operating conditions of the study.

P_N, bar	T_N, °C	ϑ,°
40	160	92.2+/-8.2
	140	95+/-9.1
	110	90.7+/-4.2
20	110	82.1 +/- 8.1

Table 7. Spray geometry for acetone in different operating conditions.

	ACETONE			METHANOL	ETHYL ACETATE	METHYL ACETATE
T_N, °C	110	140	160	110	110	110
$\dot{m}_V$, kg/m^2/s	16.9	31.9	46.4	9.3	14.4	21.5

Table 8: calculation of the evaporation mass flux $\dot{m}_V$ at initial condition

	ACETONE	METHANOL	ETHYL ACETATE	METHYL ACETATE
T_N, °C	110	110	110	110
$\dot{m}_V$, kg/m2/s	16.9	9.3	14.4	21.5
X_{vap}	0.55	0.36	0.63	0.59

Table 9: calculation of the evaporation mass flux m_V at initial condition